SHORT PERIOD BINARY STAR FORMATION: SIMULATING THE FISSION MODEL WITH THE ADDITION OF LARGE CIRCUMSTELLAR DISKS

by

CARL RANNEY

A THESIS

Presented to the Department of Physics
and the Robert D. Clark Honors College
in partial fulfillment of the requirements for the degree of
Bachelor of Science

June 2018

An Abstract of the Thesis of

Carl Ranney for the degree of Bachelor of Science in the Department of Physics to be taken June 2018

Title: Short Period Binary Star Formation: Simulating the Fission Model with the Addition of Large Circumstellar Disks

Approved: _____

Doctor James Imamura

The purpose of this research is to determine the validity of the fission model of short orbital period binary star formation. The fission model describes the process in which a protostar with a rapid rotation splits into two bodies which then orbit around a common center of mass. The fission model is one of the three major models currently under investigation by the wider astrophysical community as possible sources for the formation of short orbital period binary star systems. While fission has not received much attention in the last two decades due to results found in large scale numerical simulations, the advances in computational power now available allow much more complex simulations that show promise in solving this problem. Rather than looking at single stars, we are simulating the evolution of a rotating protostar with a large circumstellar disk that is approaching a reverse Roche limit, where the mass of the disk starts to pull the protostar apart. By including this large disk in our calculations, we find that the prospects for fission are greatly enhanced. We use the computer code Chymera in ACISS and Talapas, the University of Oregon high-performance computing clusters in our study to simulate the fluid dynamics of this system. Unsurprisingly, our nonlinear simulations of solitary stars show no fission occurring, but out linear simulations with large circumstellar disks show greatly decreased growth rates, allowing for the possibility for fission as these instabilities build. Our nonlinear simulations of these systems are inconclusive, but promising.

Acknowledgements

I would like to thank Professor James Imamura for the tremendous amount of effort he has put into this project. He has really gone above and beyond what was called for, and I appreciate his commitment. I would also like to thank Stan Micklavzina. He has been a mentor to me throughout my time at the University of Oregon, and I appreciate his help and support. I would like to make special note of Professor Susanna Lim from the Clark Honors College who took over the position of Honors College Representative on my Thesis Committee at the last minute. I am thankful for her understanding. Lastly, I would like to thank my friends and family for their support throughout this project. There help has been invaluable, as well as their willingness to prod we back into motion when I started to stall out. Even if I did not always say it, I appreciative for your efforts.

Table of Contents

List of Accompanying Materials

1. Animated Density Plots for Single Rotating Stars
2. Animated Density Plots for Star Disk Systems

List of Figures

List of Tables

Definitions

Throughout this paper, I will use many terms that are not common in normal conversation. For this reason, I included several definitions that might prove useful.

Star:
For the purposes of this paper, a star is a stellar body capable of initiating nuclear fusion in its core.

Interstellar Clouds:
Interstellar clouds refer to regions of accumulated gas and dust, which are the initial stage of star formation.[1]

Protostar:
A protostar is the pre-nuclear burning object, which often results in a star.[2]

Binary Star:
A binary star is a system of two stars in orbit about a common center of mass.[3]

Celestial Body:
Any stellar object, from a grain of dust to a galaxy, outside of the Earth's atmosphere is referred to as a Celestial Body. This is often shortened to "body".

Circumstellar Disk:
A circumstellar disk is a large disk of gas and dusk that forms around a protostar during its initial collapse stage. This material is what eventually forms planets and other stellar objects in orbit around the star. A lot of this material is also blown away by stellar radiation.

Period:
When discussing binary stars, the period of the system refers to the time it takes for the star to make one complete rotation about their center of mass.

Short Period Binary Star:
A binary star system with a separation of less than a few Solar Radii, or alternatively with an orbit that takes less the a few days to traverse.

1 Carroll, Bradley W., and Dale A. Ostlie. An introduction to modern astrophysics. Harlow: Pearson, 2014, P.406.
2 Carroll, Bradley W., and Dale A. Ostlie. An introduction to modern astrophysics. Harlow: Pearson, 2014, P.412.
3 Carroll, Bradley W., and Dale A. Ostlie. An introduction to modern astrophysics. Harlow: Pearson, 2014, P.108.

The Solar Unit:
A solar unit is often used when talking about the properties of stars, and other stellar objects. They are simply a comparison of the properties of an object to those of the sun. Thus, an object of three solar masses ($3M_{\odot}$) is simply three times the mass of the sun. Similarly, an object with one half solar luminosities ($\frac{1}{2}L_{\odot}$) has one half the luminosity of the sun.

The Light Unit:
A light unit is a unit of distance measured by the distance traveled by light in a vacuum in a given period of time. Thus, a lightyear is the distance light travels in a year, while a light second is the distance traveled in one second. One light year is 9.4607×10^{12} km.

The Astronomical Unit (AU):
The astronomical unit is often used to indicate distances in systems of interacting stellar bodies. It is simply referring to the average distance separating the sun and the earth. Thus, an object orbiting 30 AUs from a common center of mass is 30 times the distance of separation between the sun to the earth. For reference, Pluto's average distance from the sun is 39.5 AU, or 0.0006226 light years.

Conservation of Angular Momentum:
The conservation of Angular Momentum is a fundamental law of physics, and states that unless acted on by a torque, the angular momentum of a system must remain constant.

Isothermal:
An isothermal process is a changing system, in which the temperature remains constant. (i.e. if an interstellar cloud shrinks, but stays at the same temperature, it is an isothermal collapse or contraction.)

Adiabatic:
An adiabatic process is one that occurs at a constant entropy (i.e. if an interstellar cloud shrinks, but retains all of the work from compression, it is adiabatic.)

Kelvin:
The Kelvin temperature scale is closely related to the Celsius scale but is defined so that zero degrees Kelvin is the absolute coldest any object can be.

Equilibrium:
In thermodynamics and chemistry, equilibrium refers to the state at which all opposing forces and influences inside of a system are balanced. For example, if two objects of different temperature were brought into contact, the equilibrium temperature would be reached when there was no longer any flow of heat between them and were thus at the same temperature somewhere between the two original temperatures.

Tidal Forces:
Tidal forces are differential forces. For example, differing strength of the gravitational attraction between two closely interacting celestial bodies leads to tidal forces. This can be seen in the tides in Earth's oceans, which are caused by the tidal interactions between the Earth and the Moon.

Bifurcation:
Bifurcation is the splitting of a main body into two parts.

The H-R Diagram:
A type of graph often used in astrophysics to display the properties of stars, and other stellar objects. The H-R diagram is usually displayed with the absolute magnitude (brightness) on the vertical axis (with brightness increasing upward), and the spectral type (types O, B, A, F, G, K and M) on the bottom (with temperature increasing to the left). Spectral type in this instance refers to the Harvard classification scheme, which determines the temperature of a star based on its hydrogen spectral lines. Often, the luminosity is used instead of absolute magnitude, but they refer to the same thing, and spectral type is almost always shown alongside the surface temperature of the star in Kelvin. This is because, while spectral type is relatively easy to determine, it is not very useful in most calculations.

Model:
A representation of an idea, an object, a process or a system that is used to describe and explain phenomena that cannot be experienced directly.

Reverse Roche Limit (RRL):
The Roche limit is where the tidal forces acting on an orbiting body become so great that it is ripped apart. This is most commonly seen in studying the formation of Saturn's rings. The reverse Roche limit is where a ring orbiting a body is so massive that the central body is torn apart.

Chapter 1: An Overview of Binary Star Formation Models and their History

Part 1: The Importance of Understanding Binary Star Formation

To any astrophysicist, it is enough to look at the problems in our current model of binary star formation and say that they need to be solved. However, this does not explain why it should be important to other disciplines. A historian, or political science major might look at this problem and see nothing more than an academic exercise. However, this strikes at the core of why people study science at all. During Einstein's time, it was generally thought that all of science had been discovered, with only minor inconsistencies to be ironed out. One such inconsistency was a slight deviation between the model of Mercury's orbit based on Newton's laws, and the observed data. This inconstancy is what drove Einstein to postulate his own theory of special and general relativity, which not only opened up an entire new field of study in Physics but is also critical in many modern technologies including the Global Positioning System (GPS). Without taking the effects of special and general relativity into account, the finest resolution we could achieve with these satellites would be in the order of kilometers, rather than meters.[4] In part because of this discovery, as well as the breakthroughs in quantum mechanics, the scientific community's conception of our understanding of the universe has fundamentally shifted. The scientists of the late 1800s viewed the tapestry of science as an almost complete work of art, with only small corrections to look forward to. Now, we view our understanding as a collection of small bubbles slowly

[4] Ashby, Neil. "Relativity in the Global Positioning System." *Living Reviews in Relativity* 6, no. 1 (2003). doi:10.12942/lrr-2003-1.

expanding outward with each new correction to our model, and sometimes connecting in unexpected ways. While it is much more likely that the case I will be looking at will not have such a profound impact on the field, it is crucial to look at all such inconstancies we find, because we never can tell which requires a simple correction, and which will fundamentally change the way we view the universe.

Part 2: Basic Star Formation and Stellar Structure

While the specifics of short period binary star formation are currently unknown, the models used to predict the formation of non-rotating stars is very well understood and is very important to understand if one hopes to understand the mechanics of more complex systems. The most widely accepted theory on the subject is known as the nebular hypothesis, proposed in 1755 by Immanuel Kant.[5] This theory postulates that all stars form from interstellar clouds which have exceeded what is called the Jeans Mass and Jeans Radius, or have been subject to an external pressure such that the critical mass needed to induce gravitational collapse is reduced to what is called the Bonnor-Ebert mass. The equations for the Jeans Mass, Bonnor-Ebert Mass and Jeans Radius can be seen in equation 1 and 2. Once the process of gravitational collapse has begun, the cloud will simply follow the free-fall timescale. The equation for free-fall of an interstellar cloud can be seen in equation 2. Since this timescale does not depend on the radius of the cloud, so long as the initial density of the cloud is uniform, the density will increase at the same rate throughout the body. The moment the mass in a cloud exceeds the Jeans Mass that a cloud qualifies as a protostar, but the effect does not

[5] Carroll, Bradley W., and Dale A. Ostlie. *An introduction to modern astrophysics*. Harlow: Pearson, 2014, P. 405.

become visible until collisions between individual particles increases the internal pressure and temperature of the body enough to start to slow the collapse. This heating and compression at the core of the protostar is what eventually leads to high enough temperatures to initiate hydrogen fusion, thus fitting our definition of a star. The evolutionary track of an evolving protostar on the H-R Diagram can be seen in figure 1.

$$M_J \cong \left(\frac{5kT}{G\mu m_h}\right)^{3/2}\left(\frac{3}{4\pi\rho_0}\right)^{1/2} \quad (1)$$

$$R_J \cong \left(\frac{15kT}{4\pi G\mu m_H \rho_0}\right)^{1/2} \quad (2)$$

$$M_{BE} = \frac{c_{BE}v_T^4}{P_o^{1/2}G^{3/2}} \quad (3)$$

$$v_T = \sqrt{kT/\mu m_h} \quad (4)$$

where M_J is the Jeans Mass, R_J is the Jeans Radius, M_{BE} is the Bonnor-Ebert Mass, and v_T is the isothermal sound speed. The constants seen in these equations are; k, the Boltzmann constant, T, the temperature in kelvin, G, the gravitational constant, μ, the mean molecular weight, m_H, molecular weight of Hydrogen, ρ_0, the internal mass density of the cloud, P_0, the eternal compression force, and c_{BE}, a dimensionless constant approximately equal to 1.18.

$$t_{ff} = \left(\frac{3\pi}{32}\frac{1}{G\rho_0}\right)^{1/2} \quad (5)$$

where t_{ff} is the Free-Fall Timescale, and G and ρ_0 are the same variables as previously mentioned.

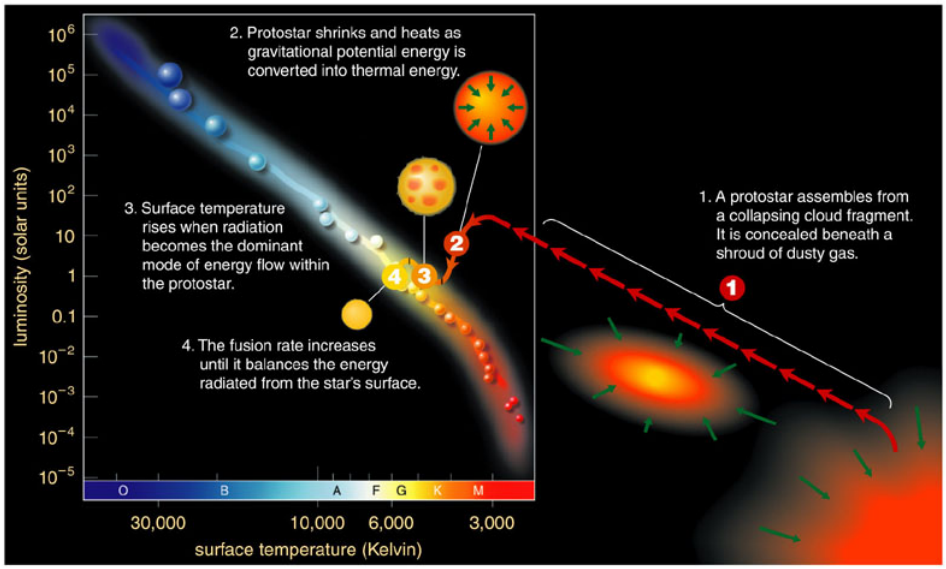

Figure 1: Pre-Main Sequence Stellar Evolution

In this H-R diagram we see that as the interstellar cloud contracts, its surface temperature and luminosity also increase. However, as radiation from nuclear fusion in the core begins to dominate the energy output, the luminosity will decrease. This will continue until the energy rate being generated in the core is equal to the energy loss at the surface.

While the models used to predict the birth of stars is very well understood and accepted by the vast majority of the astrophysical community, we still have very little observational data of stars in this stage of their development. By using the free-fall formula, we are able to find a rough timescale of pre-stellar evolution of about 10,000 to 100,000 years. This may seem like a lot of time, but when looking at stellar objects that can last billions of years or even trillions of years, it is unsurprising that we have very little observational data showing the very early stages of their evolution. This is not even taking into consideration how dim these objects are in comparison to other stellar bodies. However, we are able to tell a lot about how these systems should evolve

by the end results. It has been widely accepted for a long time that the majority of stars in the Milky Way are part of binary star systems. In fact, in our stellar neighborhood, about 60 percent of all stars are part of multi-star systems.[6] Since there is no reason to believe that the Milky Way is unique in this phenomenon, we must therefore conclude that a statistically significant number of stars in the universe are part of binary systems. What is perhaps more significant in this paper is that the ages of these binary systems are consistent with models assuming that the stars formed together, rather than forming separately, and becoming locked together later in life. This tells us that it is imperative to our model of stellar formation to include some capability to form these multi-star systems.

The earliest such model was envisioned by Pierre-Simon Laplace in 1796.[7] The model was initially very crude but was later refined by Kelvin and Tait in 1883. This model postulates that as a large, slowly spinning, gas cloud began to collapse it would start to spin faster due to the effects of the conservation of angular momentum. Given that these clouds could be anywhere from one to ten lightyears across when first beginning to form and end up as stars only a few light seconds across, even very slowly spinning clouds can end up as very quickly spinning objects. This model depended on the fact that many of these would result in stars spinning far too rapidly to be stable. As the protostar continued to collapse, the forces exerted on the collapsing sphere would cause the object to undergo what is called bifurcation, which can be seen in figure 4. As the object reached different points of instability it would continue to bifurcate, until it

[6] Schulz, Norbert S. From dust to stars: studies of the formation and early evolution of stars. Berlin: Springer, 2007, P. 141.
[7] Kondo, Yoji, Ronald Sylvester. Polidan, and Roberto SisterÓ. Evolutionary processes in interacting binary stars: proceedings of the 151st Symposium of the International Astronomical Union, held in Cordoba, Argentina, August 5-9, 1991. Dordrecht: Kluwer academic publ., 1992.

reached a point where it would fission into two objects orbiting each other at a short period. This model was also used to explain the formation of an excretion disk, and planets.[8] This was a very widely accepted theory for a very long time, but unfortunately could not be proven because of a lack of adequate computing capability. However, in the 1990's, a team was able to accurately model the theory, and found that instead of further bifurcation, the protostar developed two bulbs, which flung off low mass, high velocity particles. This loss of mass was enough to deplete the angular momentum of the system to such a point that the protostar could re-stabilize. It is now unclear exactly how these systems are able to form.

8 Carroll, Bradley W., and Dale A. Ostlie. An introduction to modern astrophysics. Harlow: Pearson, 2014, P. 425.

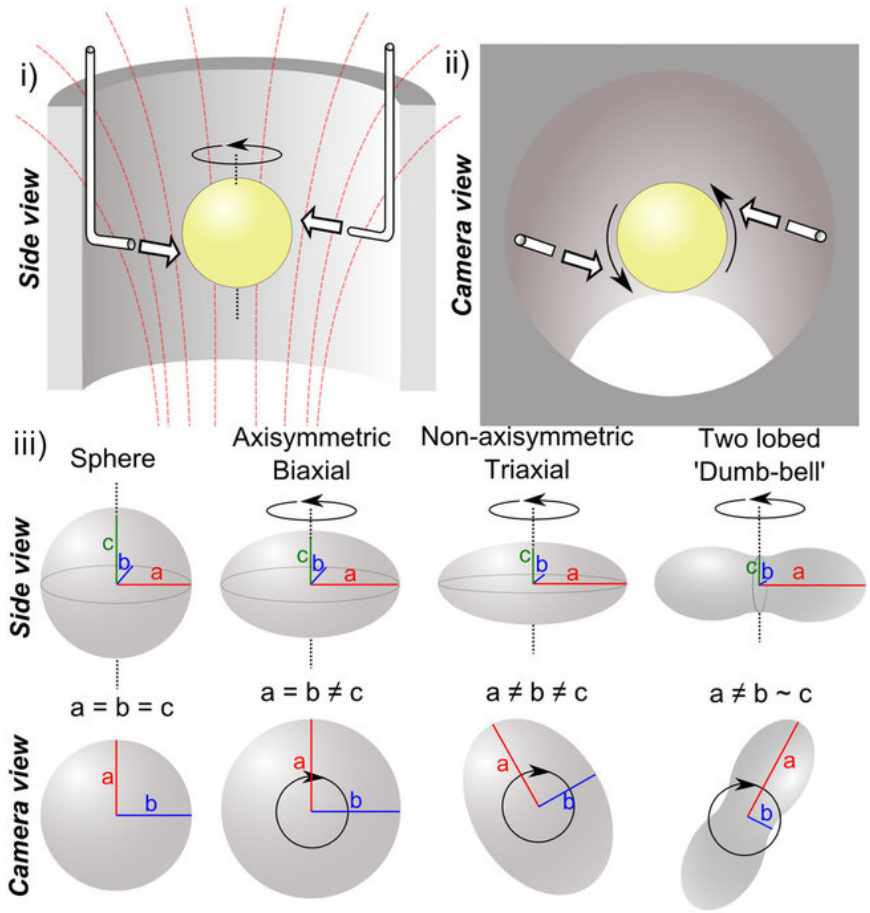

Figure 2: Simple Bifurcation of a Rotating Sphere

This figure shows the process of bifurcation. According to Laplace, Kelvin and Tait, this should eventually lead to fission of the object.

Part 3: The Three Models

When considering the formation of binary star systems, we see three major competing theories. These are fission, fragmentation and capture. The fission process is the model proposed by Laplace described above. Fragmentation has many of the same properties of fission but is described as splitting much earlier in the protostar's development. Thus, rather than collapsing into one quickly rotating sphere, the cloud will form two separate nodes, orbiting about each other with a very long period. The last model is that of capture. This idea suggests that stars which formed close together

can become locked, if effected by a third body (i.e. another stellar object). Alternatively, tidal forces between the stars, or the stars accretion disc could also be used to lose enough energy to become locked. These processes can be seen in figure 5. These theories all have at least some data supporting their claims. However, the true model is most likely is a combination of all of these effects. However, for the purposes of this project I will be postulating that all short period binaries are formed through fission, rather than the other two methods. However, it is important to understand the strengths and weaknesses of all three of these models, so I will be going over research done on all three.

Part 4: The Capture Model

Capture was first proposed as a serious contender in binary star models by Stoney in 1867, and has a large variety in its specifics, which has allowed it to retain a lot of support. The process of capture is described as,

> "Two independently formed stars [captured] into orbit if (1) a third body is present to take away the excess energy, if (2) the encounter is close enough so that tidal dissipation preforms the same function, or if (3) a dissipative medium, such as residual gas in a young cluster, is present."[9]

While the capture model has historically received a lot of attention, it is unlikely that these processes account for a large percentage of the total binary systems. This is because the bodies involved in these models must be very close to one another. The equations modeling which captures are possible can be seen here.

$$R_d \sim \frac{GM}{v^2} \tag{6}$$

[9] Kondo, Yoji, Ronald Sylvester. Polidan, and Roberto SisterÓ. Evolutionary processes in interacting binary stars: proceedings of the 151st Symposium of the International Astronomical Union, held in Cordoba, Argentina, August 5-9, 1991. Dordrecht: Kluwer academic publ., 1992, P.11.

$$R_d \sim (2 \; or \; 3) R_s \tag{7}$$

Where R_d the radius of dynamic capture, G is the gravitational constant, v is the velocity dispersion, R_t is the radius of the sphere being tidally captured, and R_s is the radius of the stellar body. Specifically, the gravitational constant is, $G = 6.67 \times 10^{-11} \, N \cdot m^2 \cdot kg^{-2}$ Note that the radius of dynamic capture is usually around 1,000 A.U. and the radius of tidal capture is usually less then 1 A.U. These close encounters are relatively uncommon even in clusters of new stars but is almost impossible for solitary stars. For instance, the sun's closest neighbor is the Alpha Centauri system (a three-star system), which is 4.37 lightyears from us. This is 276,363.5 A.U.

Because of these restraints, it is very unlikely that a solitary star would ever be close enough to another star for any form of capture to occur. Advocates of the model instead propose that binaries primarily form in stellar clusters, where the large number of stars would lend itself to many of these interactions occurring. This would also explain why the stars were the same approximate age, since stars in stellar clusters all form at about the same time. However, with the recent discovery of planetary systems orbiting multi-star systems, it is becoming increasingly unlikely that capture makes up any significant percentage of binary star formation.

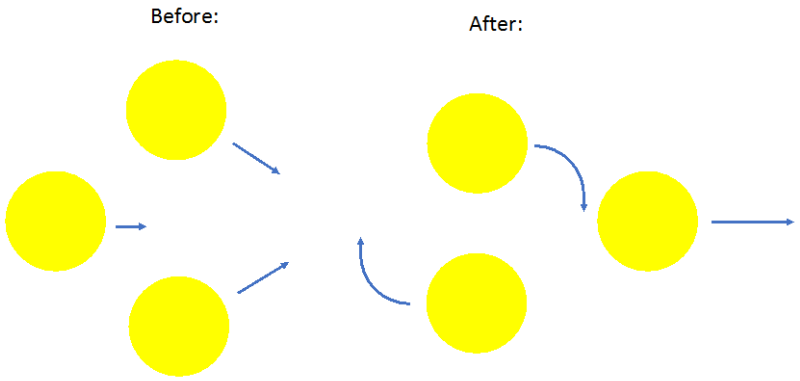

Figure 3: Three Body ‘dynamic capture’

Notice that the arrow showing the velocity of the third interacting body becomes longer after the interaction. This is to indicate that it has gained energy from the exchange, thus allowing the other two bodies to remain in the zone of gravitational interaction.

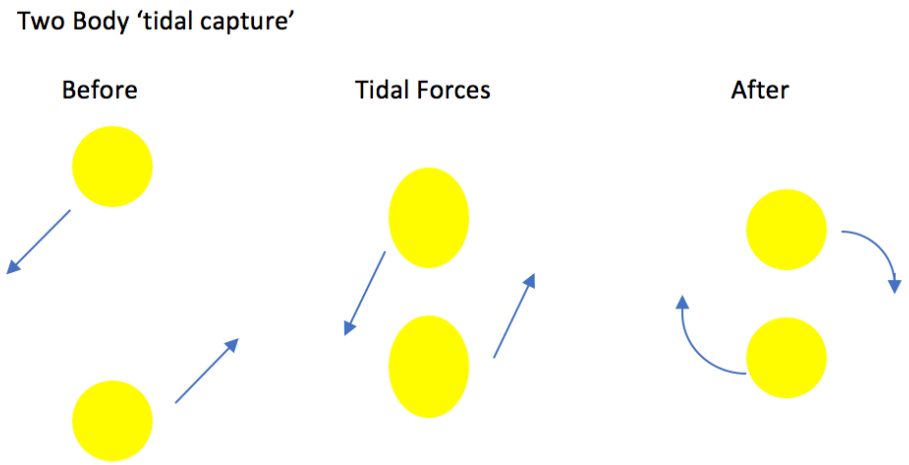

Figure 4: Two Body ‘tidal capture’

Notice that, in this system, rather than losing energy to a third body, the orbital velocity is lost to tidal forces.

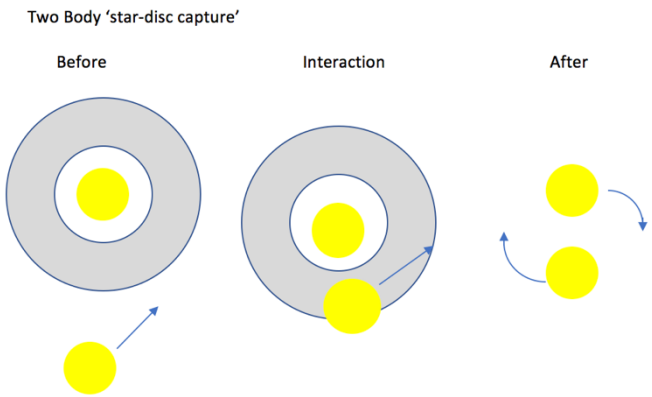

Figure 5: Two Body 'star-disk capture'

In star-disk capture, the tidal forces of the stellar disk of a star will covert enough energy in this system to allow for capture to occur.

Part 5: The Fragmentation Model

The fragmentation model is currently the most widely accepted theory of binary star formation, with work done by the likes of Boss, Miyama, Tohline and Burket, just name a few.[10] While conceptually similar to the fission model, the idea of fragmentation can be much more responsive to changes in initial conditions. Because of this there are several models for how fragmentation can occur. The simplest of these models is the prompted initial fragmentation model, which has been extensively researched by Pringle in 1989.[11] In this model, the initial cloud is made up of several Jeans Masses in an unstable state. Simulations of this model have been very successful in showing long period binaries but have been criticized for their unreasonable starting conditions. The second model is that of fragmentation during collapse, which has been advocated by Boss in a number of papers.[12] This model starts with a mild Jeans instability, such has a

10 Clarke, Cathie. "Theories for binary star formation." Astrophysics and Space Science 223, no. 1-2 (1995): 76. doi:10.1007/bf00989156.
11 Pringle, J. E. "On the Formation of Binary Stars ." Monthly Notices of the Royal Astronomical Society 239 (July 18, 1989): 361-70. doi:10.1093/mnras/239.2.361.
12 Collapse and Fragmentation of Rotating, Adiabatic Clouds

slight difference in pressure across the initial cloud. As the cloud collapses, it will slow due to centrifugal forces because of its increased angular velocity. It is postulated that at this point the cloud is able to collapse into two separate protostars, which orbit each other at this point. This model does have its problems, as it relies on isothermal heat exchange, which only hold true until the density of the protostar reaches about ~10^{-14} g cm^{-3}. [13] After this point the gas cannot cool quickly enough, and thus becomes adiabatic, which enhances the effects of pressure gradients. This will generally occur at a distance of several A.U. and is why many believe that short period binary star formation is impossible to simulate with this model. The last model commonly associated with fragmentation is fragmentation after collapse. This model has mostly been supported by Adams and Shu in papers published in the 1990's.[14] In the model, they looked at the possibility of fragmentation in a system which had already become adiabatic but had then heated enough for the hydrogen atoms in the cloud to dissociate (or have broken all chemical bonds in the cloud and separated all the atoms). This would temporarily cause the cloud to revert to an isothermal system, which could theoretically fragment. Unfortunately, there has been very little evidence to support this happening.[15]

Part 6: The Fission Model

The idea of the fission model has been around since the late 1700's and has survived relatively unchanged since that time. This is because of its relatively simple

[13] Clarke, Cathie. "Theories for binary star formation." *Astrophysics and Space Science* 223, no. 1-2 (1995): 78. doi:10.1007/bf00989156.
[14] Sahade, J., G. E. McCluskey, and Y. Kondo, eds. *The Realm of Interacting Binary Stars*. Vol. 177. Springer Netherlands, 1993, P.377.
[15] Clarke, Cathie. "Theories for binary star formation." *Astrophysics and Space Science* 223, no. 1-2 (1995): 80. doi:10.1007/bf00989156.

premise. The entire idea is centered around the behavior of incompressible fluid, which is well known to exhibit this behavior on smaller scales. The theory states that once the protostar has shifted from a collapsing cloud to a structure supported by internal pressure, the rotational instability caused by its fast rotation would cause the object to quickly bifurcate, and eventually fission. This idea is particularly important in the creation of short period binaries, with periods of less than a few days.

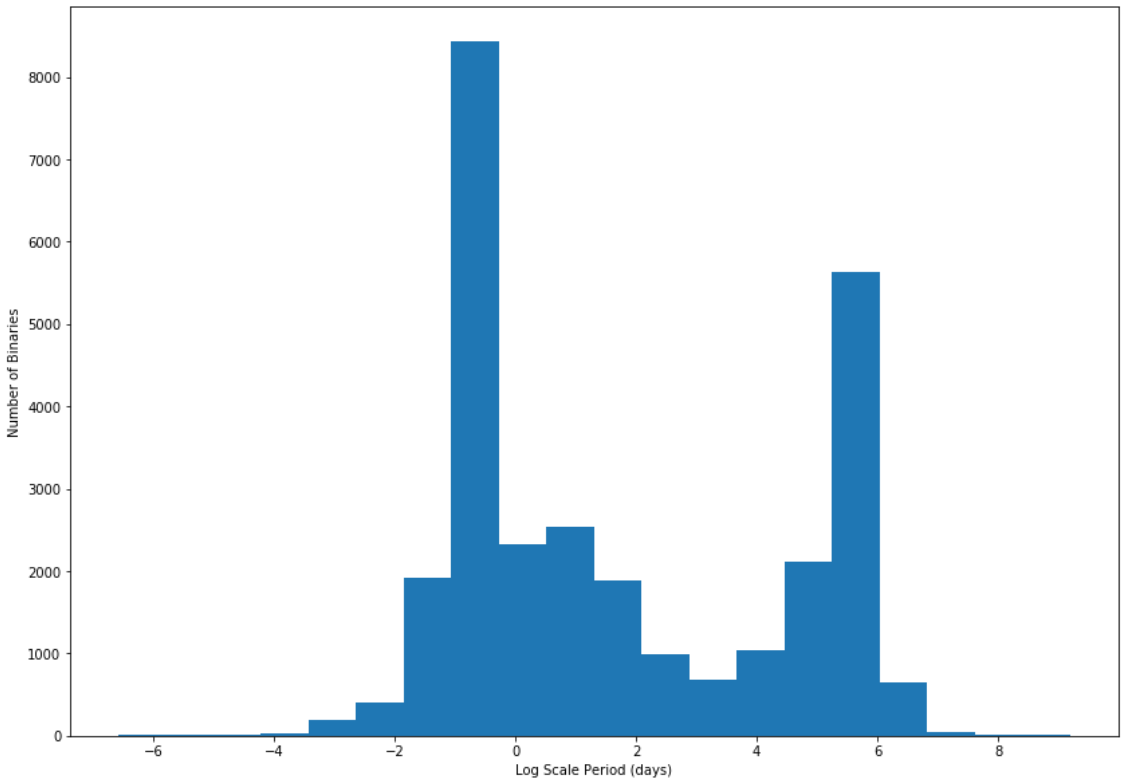

Figure 6: Log Scale Period Distribution of Binary Systems

In this plot we see the distribution of binary periods in the 2017 version of the General Catalog of Variable Stars (GCVS). Anything under a $10^1 = 10$ day period is considered a short period binary.

The other models described above have a lot of trouble simulating the formation of these systems, and as we can see in the figure above, these make up a large portion of

the total binary population. For many, the fission model offers the only reasonable answer to how these systems form.

However, despite this relatively simple premise there is little evidence in simulations that this can actually occur. In the 1990's a comprehensive simulation was designed to test the model but failed to produce the desired effect. Instead of cleanly separating into two objects orbiting a common center of mass, the star warped into a 'peanut shape' and flung small particles of matter from the lobes at high velocities. An illustration of this effect can be seen in figure 7 (P.27). Even though the particles had a low overall mass, the high velocity was able to give the particles a large radius, thus effectively lowering the angular velocity of the star until it was able to stabilize. Despite these failures, the model still has support. As stated by Cathie Clarke in *Theories for Binary Star Formation*,

> "Fission nevertheless continues to have its champions, less on theoretical grounds, then on the grounds that it would, in principle, allow for the formation of binaries at separations of a few stellar radii, which has long been considered difficult by other mechanisms" (P.80-81)[16]

It is my hope that my own simulation will be able to bridge the gap between simulation, and reality.

16 Clarke, Cathie. "Theories for binary star formation." Astrophysics and Space Science 223, no. 1-2 (1995): 80-81. doi:10.1007/bf00989156.

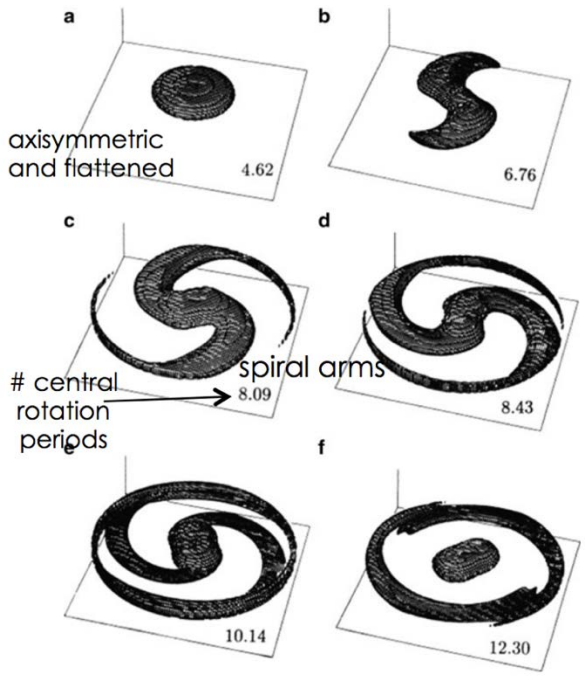

Figure 7: The Fission Model

This illustration is a somewhat exaggerated view of this result. In most simulations, the arms of the protostar are not so extensive, and the ring (if it forms at all) is not so close or as substantial.

Chapter 2: A New Approach to the Fission Model

Part 1: The Addition of a Protoplanetary Disk

As previously stated, the fission model has long been considered by most to be the least reliable of the three major models of binary star formation. While in principle, the model could account for binary systems which are difficult to explain in any other way, the existing simulations of these systems have shown very little evidence of adhering to this behavior. The reason for this is rather simple. The early versions of the fission model relied on a rotating star to act like a similarly rotating incompressible fluid. Many early astrophysicists working on this problem based their conclusions on spinning water drops, which do behave in the manner described in the fission model. However, stars do not. This makes sense, as liquid water and hydrogen plasma have very different properties. When rotated, water is not as free to warp, as it is essentially incompressible, whereas plasma is highly compressible. Thus, when rotated, the various instabilities in the stellar structure cause the star to fling small amounts of material away from the main body, thus decreasing its overall angular momentum and slowing the star enough for it to stabilize. When looked at in this light, it is obvious that this model will never work unless there is some other mechanism in place to decrease the effect of these linear instabilities and allow for the slower acting nonlinear instabilities to act on the system. While this may seem like a difficult thing to accomplish, there happens to be a mechanism around most new stars that fits our needs perfectly.

During the formation of a star, not all of the gas and dust will go into making the star. A portion of the collapsing material will be ejected from the system, sending shockwaves that can trigger other stars to form. More collapsing material will form

what is called an accretion disk or protoplanetary disk. It is the material in this disk that eventually forms the planets, comets and asteroids that make up a stellar system. It is also these disks that will hopefully hold the key to simulating a functioning fission simulation. In astrophysics, there is a term called the Roche limit, which is the closest distance a satellite can approach a planet before being ripped apart by tidal forces. It is this phenomenon that is responsible for some of the rings surrounding many of the gas giants in our own solar system. For rigid satellites, the approximate form of the equation to find this radius is,[17]

$$d = 2.44\, R_M \left(\frac{\rho_M}{\rho_m}\right)^{1/3} = 2.44\, R_m \left(\frac{M_M}{M_m}\right)^{1/3} \quad (8)$$

In this equation, 'd' is the Roche limit, R_M is the radius of the main body, ρ_M *and* ρ_m are the density of the main body and the satellite respectively, and M is the mass of each body. This is a useful relation to know when observing orbiting bodies but is not useful for this particular problem. What is interesting to look at however is the reverse Roche limit. This is where an orbiting disk becomes massive enough to overpower the self-gravitation of the main body and rip it apart. This particular result would also be less than ideal for our simulation, but with that being said, a system that is approaching that limit could work. This countering force to the self-gravitation of the main body could prove the key to allowing the subtler nonlinear instabilities to act on the rotating fluid. This will hopefully allow for the clean bifurcation we need for binary star formation.

[17] Biegert, Mark. "Roche Limit Examples." Math Encounters Blog. March 1, 2016. http://mathscinotes.com/2016/03/roche-limit-examples/.

Part 2: Equilibrium Models

In these simulations, we will be looking at rotating polytropic stars surrounded by inviscid polytropic disks. That is to say, both the star and the disk will not have heat transfer throughout their evolution, and the disk will have negligible viscosity. We will also be looking at stars with both uniform and differential rotation. Differential rotation is when parts of a sphere spin with different angular velocities and can be modeled as having the angular momentum distribution of a uniformly rotating incompressible sphere. For our simulation, the specific angular momentum distribution is given by,

$$h_M(m_\varpi) = 2.5 - 2.5(1 - m_\varpi)^{2/3} \tag{9}$$

where,

$$m_\varpi = \frac{4\pi \int_0^\varpi \varpi d\varpi \int_0^{Z(\varpi)} \rho(\vec{r}) dz}{M_*} \tag{10}$$

Here, m_ϖ is the cylindrical mass fraction, $\rho(\vec{r})$ is the mass density and $Z(\varpi)$ is the height of a star at cylindrical radius ϖ. As stated before, the disk is not expected to rotate with a large velocity but can be assumed to be the power law angular velocity distributions.

$$\Omega(\varpi) = \Omega_0 \left(\frac{\varpi}{r_0}\right)^{-q} \tag{11}$$

In this equation, Ω_0 is some constant and r_0 is the location of maximum density in the disk plane. Using these assumptions, that being the inviscid, axisymmetric, steady-state mass and momentum conservation equations are,

$$\nabla \cdot (\rho\, \vec{v}) = 0 \tag{12}$$

and,

$$\rho\, \vec{v} \cdot \nabla\, \vec{v} + \nabla P + \rho \nabla \Phi_g = 0 \tag{13}$$

where, $\vec{v}$ is the fluid velocity, $\vec{\nabla}P$ is the pressure gradient and $\vec{\nabla}\Phi_g$ is the gravitational potential gradient. We do not use the energy conservation equation in this case because we are describing the star as a polytropic fluid, where the Equation-of-state (EOS) relate the pressure and density by,

$$P = K\rho^{1+\frac{1}{n}} \tag{14}$$

In this equation, K is the polytropic constant and n is the polytropic index. To find the gravitational potential, we find solutions to the Poisson equation,

$$\nabla^2\Phi_g = 4\pi G\rho \tag{15}$$

The equilibrium equations are solved as follows. The conservation equations are first integrated once to find the star/disk equilibrium equation,

$$C = (n-1)K\rho^{1/n} + \Phi_g + \Phi_c \tag{16}$$

where,

$$\Phi_c = -\int^{\varpi} \Omega^2(\varpi)\varpi d\varpi \tag{17}$$

In these equations, C is the integration constant, and Φ_c is the centrifugal potential. We define central star families by their polytropic index and their rotational structure, while family members are defined by the ratio of the stars equatorial radius, r_e, to their polar radius, r_p. Disk families are defined by their polytropic index and their exponents, q. If we look back at equation 11, we see q is used in determining the angular velocity distribution of a disk. Disk family members are grouped by the ratio of the inner, r_-, and outer radius, r_+, of the disk. Star disk families are grouped by the ratio of the ratio of the maximum disk density, ρ_0, and the density of the stars core, ρ_c. This value is defined as, $\eta = \rho_0/\rho_c$. Star disk families are also defined by the ratio of the

equatorial radius of the star to the inner radius of the disk, r_e/r_-. We use the value η to control the ratio of the stellar mass to the disk mass, $M = M_*/M_d$, for a given ratio r_-/r_+. By specifying a value for η, we allow the star and disk to lie on different adiabats, which are the curves on a graph of pressure and temperature which show the adiabatic heating of cooling of gases. These solutions are then normalized so, the gravitational constant is equal to one, $G = 1$, the total mass in the system is equal to one, $M_* + M_d = 1$ and the polytropic index of the star is equal to one, $K_* = 1$. The polytropic index of the disk will not be equal to one, $K_d \neq 1$. We use the self-consistent field algorithm to solve equation [16] (Hachisu 1986).

For our equilibrium code, we first guess the density distributions for the star and the disk, ρ_* and ρ_d. We use these guesses to calculate the integration constants, C_* and C_d for the star and disk respectively, as well as the angular momentum normalizations for the star and disk, $\mathrm{h}_{0,*}$ and $\mathrm{h}_{0,d}$. In the case of the star, we evaluate equation 10 at the polar radius, $(\varpi, z) = (0, r_p)$, and at the equatorial radius, $(\varpi, z) = (r_e, 0)$. Since this is the surface of the star, the density of the star will be, $\rho_* = 0$. Evaluating for the angular momentum and integration constant show,

$$h_*^2 = \frac{\Phi_g(0,r_p) - \Phi_g(r_e,0)}{\Psi(0) - \Psi(r_e)} \tag{18}$$

$$C_* = \begin{cases} \Phi_g(0, r_p) + \Phi_c(0) \\ \Phi_g(r_e, 0) + \Phi_c(r_e) \end{cases} \tag{19}$$

$$\Phi_c(\varpi) = -\int^{\varpi} \Omega^2(\varpi)\varpi d\varpi = \left(\frac{h_0^2}{r_0^2}\right)\Psi(\xi) \tag{20}$$

$$\xi = \left(\frac{\varpi}{r_0}\right) \tag{21}$$

We know that h_0 is the specific angular momentum normalization, and $\Psi(\xi)$ is the dimensionless centrifugal potential. In the case of the disk, C_d and h_d are found in a similar manner, except that equation 10 is evaluated at $(\varpi, z) = (r_-, 0)$, and at $(\varpi, z) = (r_+, 0)$. Thus, we see,

$$h_d^2 = \frac{\Phi_g(r_-,0) - \Phi_g(r_+,0)}{\Psi(r_-) - \Psi(r_+)} \tag{22}$$

$$C_d = \begin{cases} \Phi_g(r_-, 0) + \Phi_c(r_-) \\ \Phi_g(r_+, 0) + \Phi_c(r_+) \end{cases} \tag{23}$$

We invert equation 10 with (C_*, h_*^2) and (C_d, h_d^2), as defined in equations 22 and 23 to find, $\rho_*,\ \rho_d,\ K_*$ and K_d. If our guesses made at the start of this simulation are consistent with these calculations, the calculations are stopped, and the model is declared converged. If not, we make a new guess for ρ_* and ρ_d, and repeat the previous calculations. We have defined consistent as the parameters, $C_*,\ C_d, h_*^2$ and h_d^2 varying by less than 1 part in 10^{10} in consecutive iterations.

This set of calculations are not very computationally intensive to perform, so I have looped this process to run through many different variations of the system parameters.

```
c dencity ratio(log change by 2 or 3)
        do 390 lgrhodisk = lgrhodisk,-1.00,0.1
         k_star = k_star_re
         j_star = j_star_re
         j_disk = j_disk_re

        do 290 j_disk = j_disk,jout-1,8
         k_star = k_star_re
         j_star = j_star_re
c equitorial stellar radius
         do 190 j_star = j_star,j_disk - 1,8
          k_star = k_star_re
c polar stellar radius
          do 90 k_star = k_star,j_star,8
c          reset all variables
           qd = qd_re
           np = np_re
           pin = pin_re
```

Figure 8: Nested Loops

In this figure we see the nested loops used in the equilibrium modeling portion of this project. As we can see, this code is written and compiled in Fortran90, and is a set of four nested do loops. The inner most loop iterates over the polar radius of the star, going from the listed minimum in our input file, to the equatorial radius of the star, making a perfect sphere. The second loop increases the equatorial radius of the star up to one less than the inner radius of the disk. Next the inner radius of the disk is increased to one less than the outer radius. Finally, the log of the density of the disk is increased from -2.30, which was our set starting point, to -1.00 to change the mass ratio of the star and the disk.

Throughout the course of this model, the polar radius, equatorial radius, inner radius of the disk, and the density of the disk are all slowly changed. This is all to help determine the reverse Roche limit that was described previously. By plotting the ratio of the star mass to the disk mass compared to the time over the angular frequency, and isolating specific sets of polar radii, we can see how changes in these features effect the overall cohesion of the star. By isolating these features, we can look at a particular family of stars to perform more substantial analysis on. It is these stars that we will look at with the inclusion of nonlinear instabilities.

Part 3: Linear Simulations

After we have completed the equilibrium models, we will look at both linear and nonlinear simulations of stars that we found interesting in the equilibrium data. For example, one of the things we expect to find is that stars will begin to become unstable in various nonaxisymmetric modes. In order to asses if a given star is stable or unstable, we will look at it in a linear simulation. Since these are so much faster than nonlinear simulations, we can perform many more of them, and chose only the most promising samples to look at in our nonlinear analysis. In a linear analysis, the equilibrium structure is slightly disturbed by a small perturbation. The small perturbation is then fallowed to see if it grows or if it damps and the system returns to equilibrium. The linearized evolution equations are found from the substitution of Eulerian perturbations of the form,

$$A = A_0 + \delta A(\varpi, z, t)e^{im\phi} \tag{24}$$

into the hydrodynamics equations. Here, A_0 is the equilibrium solution, and δA is the small perturbation in the meridional plane.[18] By keeping trans linear in δA, we observe that,

$$\partial_t \delta\rho = -im\Omega\delta\rho - \rho_0 \frac{\delta v_\varpi}{\varpi} - \delta v_\varpi \partial_\varpi \rho_0 - \delta v_z \partial_z \rho_0 - \rho_0(\partial_\varpi \delta v_\varpi + \frac{im}{\varpi}\delta v_\varpi + \partial_z \delta v_z) \tag{25}$$

$$\partial_t \delta v_\varpi = -im\Omega\delta v_\varpi + 2\Omega\delta v_\varpi - \frac{\gamma P_0}{\rho_0^2}\partial_\varpi \rho - (\gamma - 2)\frac{\delta\rho}{\rho_0^2}\partial_\varpi P_0 - \partial_\varpi \delta\Phi \tag{26}$$

$$\partial_t \delta v_\phi = -im\Omega\delta v_\phi + \frac{1}{\varpi}\partial_\varpi(\Omega\varpi^2)\delta v_\varpi - \frac{im}{\varpi}\frac{\gamma P_0}{\rho_0^2}\delta\rho - \frac{im}{\varpi}\delta\Phi \tag{27}$$

$$\partial_t \delta v_z = -im\Omega\delta v_z + \frac{\gamma P_0}{\rho_0^2}\partial_z \delta\rho - (\gamma - 2)\frac{\delta\rho}{\rho_0^2}\partial_z P_0 - \partial_z \delta\Phi \tag{28}$$[19]

[18] Catelan, P., F. Lucchin, S. Matarrese, and L. Moscardini. "Eulerian Perturbation Theory in Non-flat Universes: Second-order Approximation." *Monthly Notices of the Royal Astronomical Society*1, no. 1 (1995). doi:10.1093/mnras/276.1.39.

As we can see, the above equations are calculated in cylindrical coordinates. In these equations $\delta\Phi$ is the perturbed gravitational potential, and can be found in the linearized Poisson equation,

$$\nabla^2\left(\delta\Phi e^{im\phi}\right) = 4\pi G\delta\rho e^{im\phi} \tag{29}$$

The perturbed quantities are complex, so the physical solutions corresponds to the real components of each eigenfunction.

In these problems, the boundary conditions consist of: 1) mirror symmetry about the equatorial plane; 2) perturbed velocities in the radial and polar directions (ϖ and z), as well as changes in density ($\delta\rho$) that go to zero at the surface of the disk; and 3) perturbed gravitational potentials on the outer grid boundaries. These are computed in spherical harmonics including l-values up to 16. Using these boundaries, we find the fastest growing mode for a given value m. To compute analytically, we write the spatial derivatives as a finite difference and leave the time derivatives continuous. The equations are advanced using a fourth order Range-Kutta scheme. We perform tests with resolutions of grid size $n_\varpi \times n_z = 256 \times 256$ and 512×512.

Part 4: Nonlinear Analysis

For our nonlinear simulations we used the hydrodynamics code *Chymera*.[20] *Chymera* solves the hydrodynamic equations in their conservative forms,[21]

$$\partial_t\rho = -\nabla(\rho\boldsymbol{v}) \tag{30}$$

$$\partial_t(\rho\boldsymbol{v}) = -\nabla(\rho\boldsymbol{v}\boldsymbol{v}) - \nabla\left(\mathrm{P} + P_Q\right) - \rho\nabla\Phi_{\boldsymbol{g}} \tag{31}$$

---

[19] (Hadley et al. 2014)
[20] (Boley 2007, Boley et al. 2007)
21 Brusov, Peter N., and Paul P. Brusov. "Nonlinear Hydrodynamic Equations for Superfluid Helium in Aerogel." Physics Letters A314, no. 3 (2003): 239-43. doi:10.1016/s0375-9601(03)00877-6.

$$\partial_t \left(\epsilon^{\frac{1}{\gamma}}\right) = -\nabla\left(\epsilon^{\frac{1}{\gamma}}\boldsymbol{v}\right) + \frac{\epsilon^{\frac{1}{\gamma}-1}}{\gamma}\Gamma_Q \tag{32}$$

The above equations are the mass conservation equation, momentum conservation equation and the internal energy equation. The equations are solved on a Eulerian, cylindrical grid, where ϵ is the internal energy density, P_Q is the Von Neumann artificial viscosity term, and Γ_Q is the Richtmeyer artificial viscosity term. These are included to handle shock formation, and take the form,

$$P_Q = \rho(Q_{\varpi\varpi}^2 + Q_{\phi\phi}^2 + Q_{zz}^2) \tag{33}$$

$$\Gamma_Q = -\rho(Q_{\varpi\varpi}\partial_\varpi v_\varpi + Q_{\phi\phi}\frac{1}{\varpi}\partial_\phi v_\phi + Q_{zz}\partial_z v_z \tag{34}$$

Where,

$$Q_{jj} = \begin{cases} C_Q(\nabla v_j)^2, for\ \nabla v_j \leq 0 \\ 0\ , for\ \nabla v_j > 0 \end{cases} \tag{35}$$

and C_Q is a constant of order unity.[22] In our simulations we set $C_Q = 3$. *Chymera* solves the hydrodynamic equations using momentum densities, $T = \rho v_\varpi$ and $W = \rho v_z$, and angular momentum density, $A = \rho v_\phi \varpi$. This is all in second order in space and time.

[22] (Hawley et al. 1984)

Chapter 3: Numerical Results

Part 1: Isolated Rotating Stars

One of the key features of this study is demonstrating the effect of placing a massive disk around a central star will have on the fission process. For this reason, we felt it prudent to run at least a few baseline models showing the formation process of an isolated star. Using *Chymera* we looked at several variations of this system, as well as studying the existing literature on this topic. One idea we had was to reevaluate the fission model by running a set of simulations of a rotating solitary star. This is exactly what has been done in the past, but with the more accurate nonlinear fluid dynamics calculated by *Chymera*, and greater computation time we were interested to see if there were any substantial changes. We wanted to specifically look at three stars with similar external characteristics, but different internal structures. This is done by changing the value of n', which corresponds to the angular momentum index of the system. For our model, we decided to look at stars rotating at about $\frac{T}{|W|} = 0.3$. Here T is the rotatinal kinetic energy of the star and W is the gravitational energy of the star. We chose these values because it is generally understood that stars with a $\frac{T}{|W|}$ value that is greater then 0.28 will be unstable in the $m = 2$ mode. Thus, by starting with stars at just above this value, we will see stars that will hopefully start to evolve immediately. To get this result, we set

n'	Equatorial Radius	Polar Radius
0.0	120	26

1.0	120	12
4.0	120	30

Table 1: Starting Conditions of Solitary Stars

In this table we see the starting conditions of our solitary stars. Each star was given an initial angular momentum index, and we found the corresponding stellar structure.

With our additional initial conditions set so $n = 1.5$, $\log(\rho_{max}) = 0.0$, $del = 0.7$,$M_* = 0.0$, and the total dimensions of our plot is 256 by 256, we calculate the initial configuration of our model. We then let the system evolve over a long period of time.

Our results closely match those found in previous studies of similar systems. To see the results of these simulations we can look at a two-dimensional cross section of the density of our grid in the equatorial plane. At the start of each simulation the star appears undisturbed, spinning rapidly, and apparently without major changes. This however soon changes as small eddies start to form. From here it was originally thought the star should start to deform into a bar mode which becomes more extreme until the star fissions. However, we, as do earlier workers, do not see this clean bifurcation. In fact, only one of our simulations formed a proper bar mode. Instead, we see large amounts of matter being flung from the system in large arms, until enough angular momentum has been shed to allow the star to collapse back down into a single stable body.

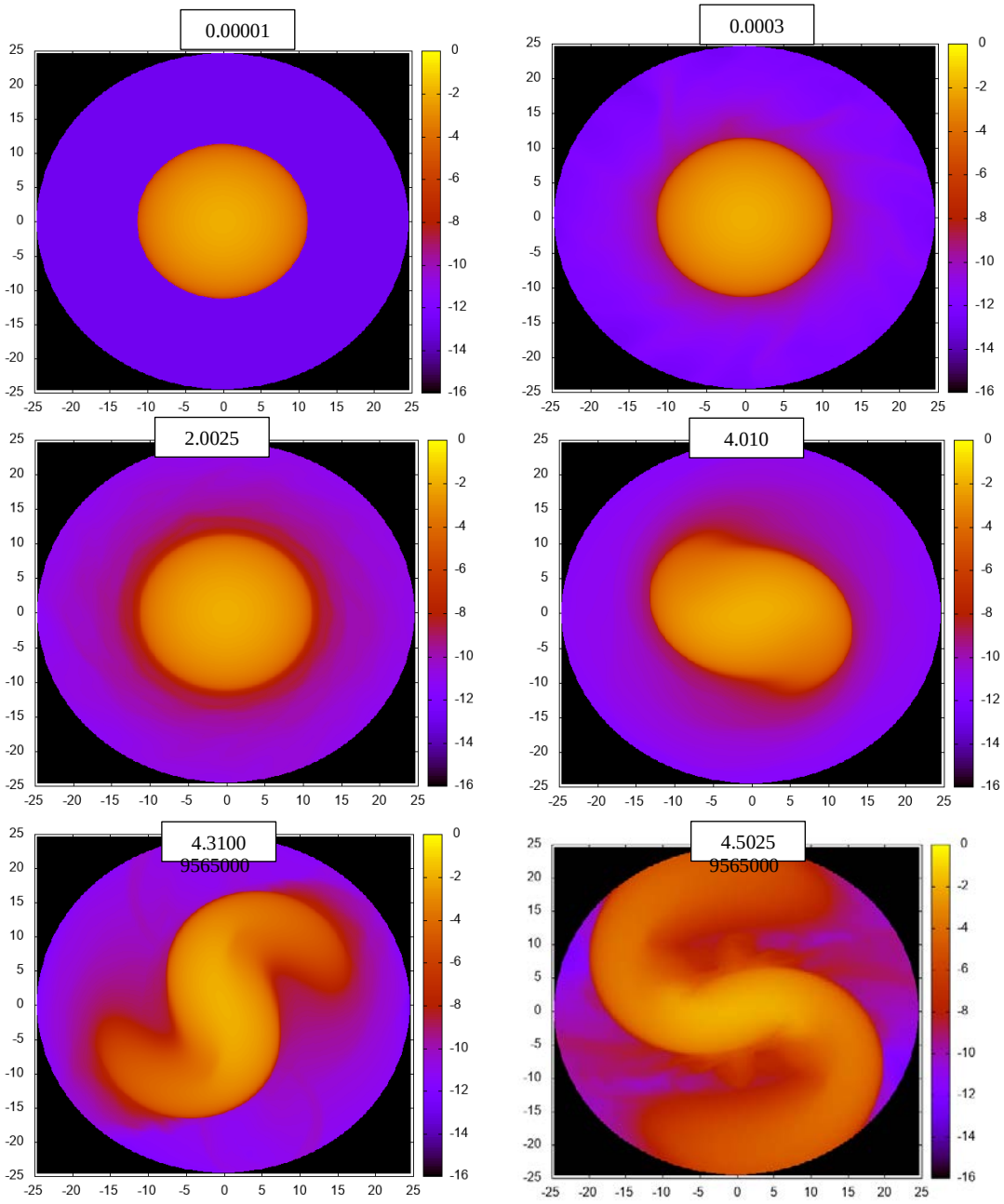
0.00001
0.0003
2.0025
4.010
4.3100
9565000
4.5025
9565000

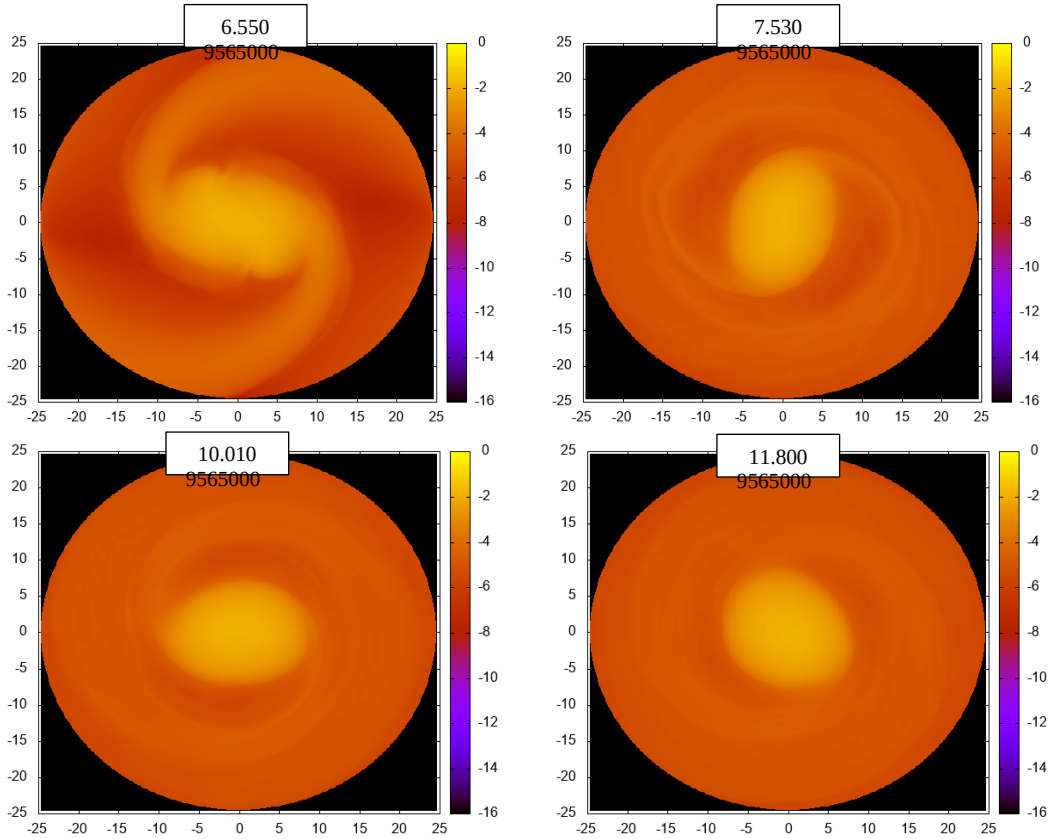

Figure 9: Rotating Star Evolution

In this sequence, we see the evolution of the n'= 0.0 system. As the star rotates, we see the formation of the bar mode that we hoped for, but instead of further bifurcation, the stars structure was ripped apart, forming large spirals. This event causes the star to lose angular momentum, allowing the star to fall back into a much more slowly rotating sphere. This overall behavior is similar to figure seven, where we saw the ejected material form a ring around the star. In the actual simulation this ring is much more diffuse, but it will likely take time for a real system to become coherent after this event.

In order to tell what is happening in these images it is helpful to look at the Fourier amplitude coefficients of each plot. We find the Fourier coefficients by fitting a Fourier series to the azimuthal structure of the density.

$$\rho(\varpi, \phi, z) = a_0^{(\varpi,z)} + \sum_{n=1}^{N} a_{n,m}^{(\varpi,z)} \cos\left(n\frac{2\pi}{m}\right) + \sum_{n=1}^{N} b_{n,m}^{(\varpi,z)} \sin\left(n\frac{2\pi}{m}\right) \quad (36)$$

where N is the number of grid cells in the azimuthal direction for each (ϖ, z) grid cell, and m is the mode number. The A_m are,

$$A_m^2 = \left(\sum_{n=1}^{N} a_{n,m}^{(\varpi,z)}\right)^2 + \left(\sum_{n=1}^{N} b_{n,m}^{(\varpi,z)}\right)^2 \tag{37}$$

This tells us which mode (m value) is dominant at any given time.

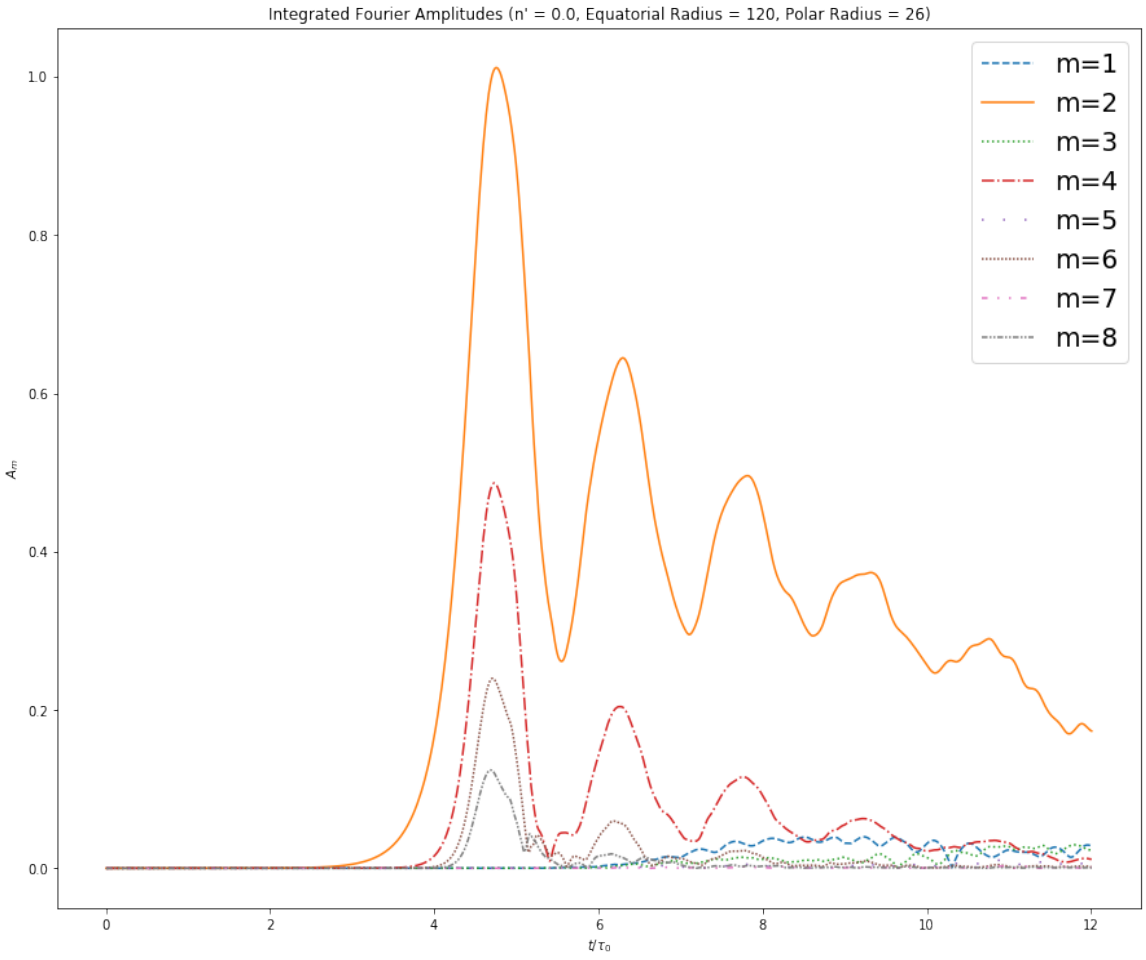

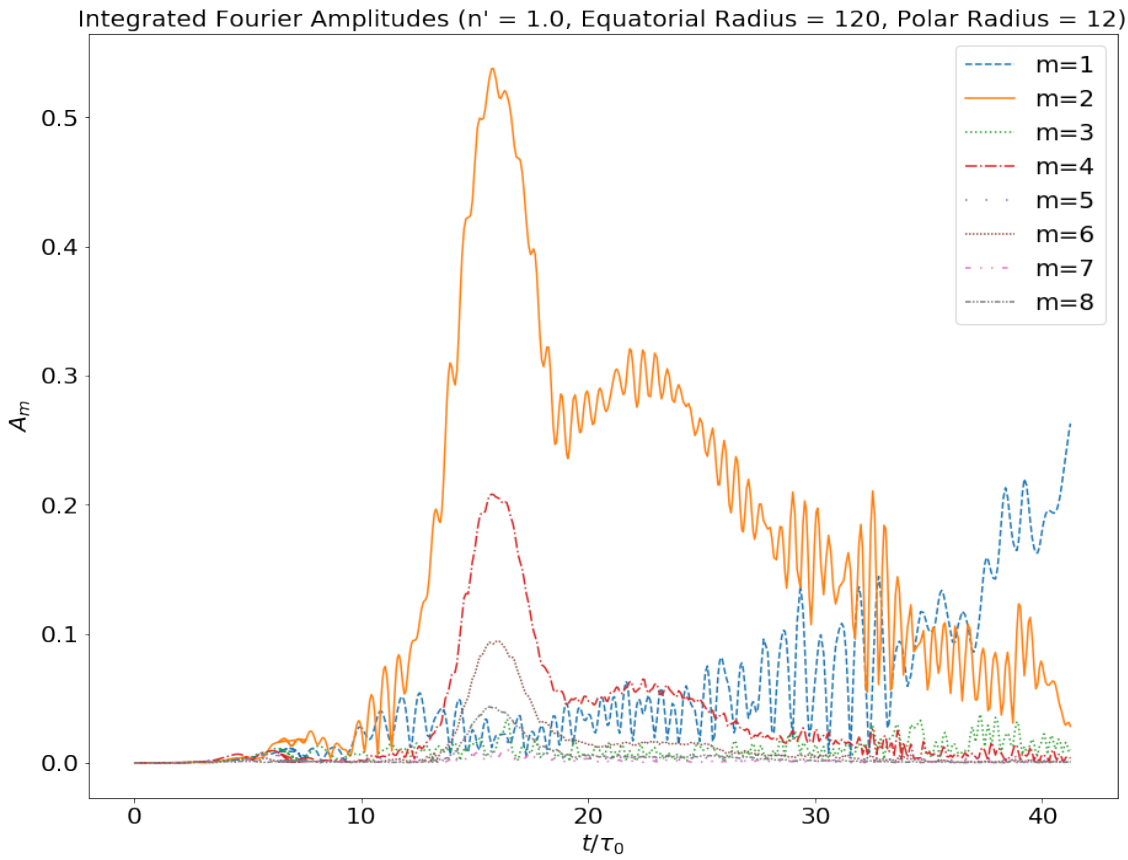
Integrated Fourier Amplitudes (n' = 1.0, Equatorial Radius = 120, Polar Radius = 12)
m=1
m=2
m=3
m=4
m=5
m=6
m=7
m=8
A_m
t/τ_0

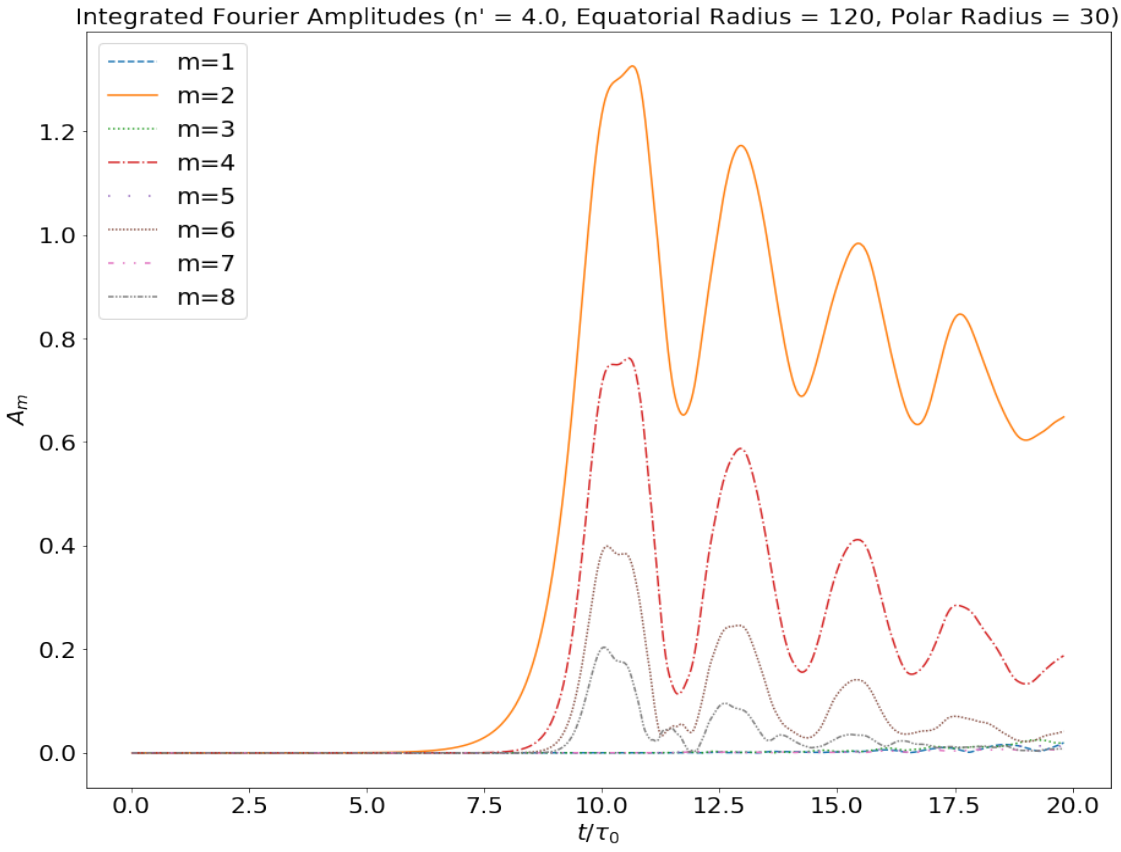
Integrated Fourier Amplitudes (n' = 4.0, Equatorial Radius = 120, Polar Radius = 30)
m=1
m=2
m=3
m=4
m=5
m=6
m=7
m=8
A_m
t/τ_0

Figure 10: Integrated Fourier Amplitudes

In this plot we see the integrated Fourier amplitudes for each of our stellar models. The Fourier amplitude A_m is the mth amplitude element of a discrete Fourier spectrum. As we can see, all three of these stars are dominated by the second order instabilities during the majority of the simulation. This is what is driving the bifurcation of the star. It is interesting to note that the n'=1.0 model starts to be dominated by the first order instabilities after the star has collapsed back down. The time scale in these plots is the time it takes for the radius of maximum density to make one orbit of the center of mass.

When we look at the Fourier plots of each solitary star, we see that all three are dominated by the $m = 2$ mode as the star starts to deform. For all models however, A_2 decreases as time increases showing that the nonaxisymmetric structure weakens as the star becomes more oblate. This makes sense as this is what we would expect in a bar mode in solitary stars. However, it is interesting to see that the $m = 4$ mode also increases more than we would expect. This could be the reason the star breaks down so quickly and is something that should be watched for in the more complicated star-disk model.

Part 2: Equilibrium Model Results

Now that we have looked at how a single rotating star behaves as it tries to reach a point of equilibrium, let us add a massive disk around the system. It is this disk, when approaching the reverse Roche limit, clean fission of a star will occur in our hypothesis. However, given the large number of parameters that this system may depend on, it becomes prudent to sample over this parameter space to find where this limit is, as well as finding appropriate samples to evaluate more completely to show if this limit even matters. In our model, we sampled over four parameters to gain an understanding of

how a disk would affect the system. The most obvious is the overall aspect ratio, r_-/r_+, of the disk. We accomplished this by changing the inner radius of the disk, r_-, while leaving the outer radius, r_+, constant. Second, we changed the size of the star. This was done by changing the equatorial radius, r_{eq}, of the star. Third, we changed the density of the disk. This changed the mass ratio of the star and the disk, without changing the fundamental geography of the system. Lastly, we would change the polar radius, r_p, of the star to change the stars overall flattening. By changing this value, we dictated how fast the star must be rotating.

In the first series of models we will sample the disk inner radius from a normalized value of 5 to 253 with a step size of 8, sample the equatorial radius from 4 to one less than the disk inner radius with a step size of 8, sample the polar radius from 4 to the equatorial radius with a step size of 8, and sample the log of the disk density from -2.23 to -1.00 with a step size of 0.1. After completing this series and plotting $\frac{T}{|W|}$ for the star versus the star to disk mass ratio, we can see a clear relationship that could easily aid in our understanding of the fission process and the reverse Roche limit. Let us look specifically at the data corresponding to stars with an equatorial radius of 84.

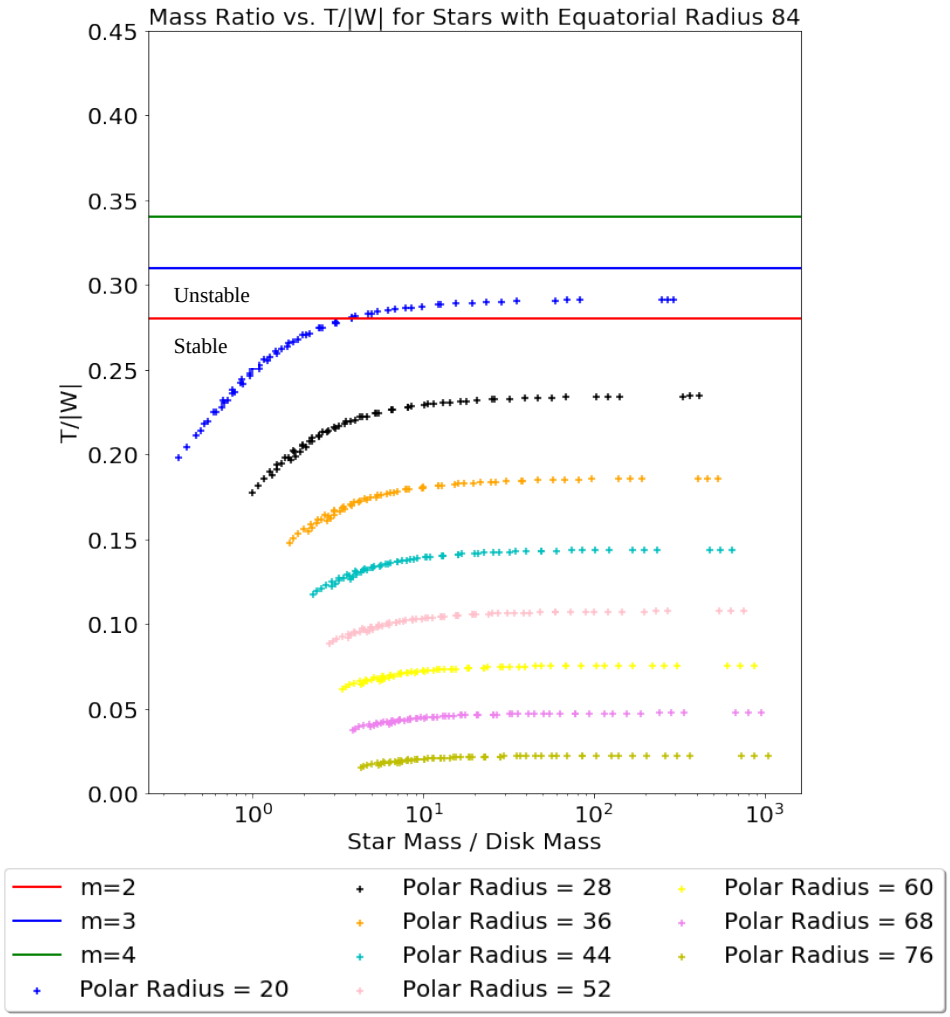

Figure 11: Isolated Equatorial Radius of 84 Plot

In this plot we see the angular velocity vs. the mass ratio of stars with an equatorial radius of 84. The distinct families of data are stars with the same polar radius. Thus, we see that the changes in each group's characteristics come from changes in the inner disk radius and density. It is this relationship that we hope will result in clean bifurcation in our proto star. The horizontal lines represent the T/|W|, or momentum density value limits for stability in spherical stars for different modes. Any values above the line will be unstable, thus, large disks driving the T/|W| value down could result in stable stars with more extreme initial conditions.

One of the key features shown in this plot is the maximum $T/|W|$ values of stable for spherical stars. We know that $T = \rho v_{\varpi}$ and W= ρv_z We see that the instability threshold for the m=2 mode is much lower than for larger values for m,

which is why the evolution of these systems is so often dominated by the m=2 mode. What is of interest to us however is the effect of increasing the size and density of the disk has on each family group. Specifically, let us look at the family group of polar radii, $R_p = 20$. For small disks, we see that this group lies above the cutoff for stability. However, as the disk size is increased, the group is driven down across this threshold. These should therefore be stable if this same limit holds true. We will need to perform linear stability calculations to see for sure.

In this figure we see several distinct family groups made up of stars with the same polar radius to equatorial radius ratio. This will give these stars the same flattening. We see that each family group approaches a value on the y-axis as the stellar mass to disk mass ratio increases, and rapidly drops as this ratio decreases. Where this line terminates at the small end of the $\frac{M_*}{M_d}$ axis where we approach the reverse Roche limit. This depends greatly on which family group are being considered. For nearly round, it is likely that the mass ratio simply cannot be lowered any more. These stars are massive enough that the disk has little to no effect on them, no matter how dense the disk. Also, the angular velocity needed to deform the star so slightly is so small compared to the amount shifted by the ring that it does not have a notable effect. For the flatter configurations however, the termination points on the left-hand side of each family group is more often the last point with a usable answer. This is the reverse Roche limit; where the effect of the disk is so great that the star is pulled apart, and thus has no angular velocity, and it is these points that we are interested in.

We can somewhat easily perform physical calculations to find this point for spherical stars surrounded by a disk, while not as rigorous as the calculations made in

the equilibrium code, it is a good way of showing that the code is not erroneous, since the values should at least be close. To that end, let us calculate this termination point for a star-disk system.

The gravitational potential of a sphere is easy to calculate. In the case of gravity, the potential is defined by the equation,

$$\Phi(r) = \frac{W}{m} = \frac{1}{m}\int_{\infty}^{r} \vec{F} \cdot d\vec{r} = -\frac{1}{m}\int_{\infty}^{r} \frac{GmM}{r^2} dr \tag{38}$$

If we define the density of the star to be uniform and set $\Phi(\infty) = 0$, we can further refine this equation to,

$$\rho(r) = \begin{cases} \gamma & for\ r \leq R_* \\ 0 & for\ r > R_* \end{cases} \tag{39}$$

$$\Phi_0(r) = -\frac{4\pi G\gamma}{r}\int_0^r r'^2 dr' - 4\pi G\gamma \int_r^{R_*} r' dr' \tag{40}$$

for $r \leq R_*$, and

$$\Phi_0(r) = -\frac{4\pi G\gamma}{r}\int_0^{R_*} r'^2 dr' \tag{41}$$

for $r > R_*$. In this case, $\Phi(r)$ is the gravitational potential, W is work, G is the gravitational constant, m and M are the masses of two interacting objects, $\rho(r)$ is the density distribution, γ is some constant, R_* is the radius of the star and r' is the reference vector for the star. We integrate these to find,

$$\Phi(r) = \begin{cases} -\frac{2\pi G\gamma}{3}\left(3{R_*}^2 - r^2\right) & for\ r \leq R_* \\ -\frac{4\pi G\gamma}{3}\frac{{R_*}^3}{r} & for\ r > R_* \end{cases} \tag{42}$$

We can also define the mass of the system as, $M = \frac{4\pi}{3}{R_*}^3\gamma$, so the potential can be redefined as,

$$\Phi(r) = \begin{cases} -GM\frac{\left(3{R_*}^2 - r^2\right)}{2{R_*}^3} & for\ r \le R_* \\ -\frac{GM}{r} & for\ r > R_* \end{cases} \quad (43)$$

This tells us the gravitational potential of a sphere, but the disk is much harder to calculate. We can simplify this problem greatly by taking the disk to be an infinitely thin ring and calculating the potential inside the ring at an arbitrary point.[23]

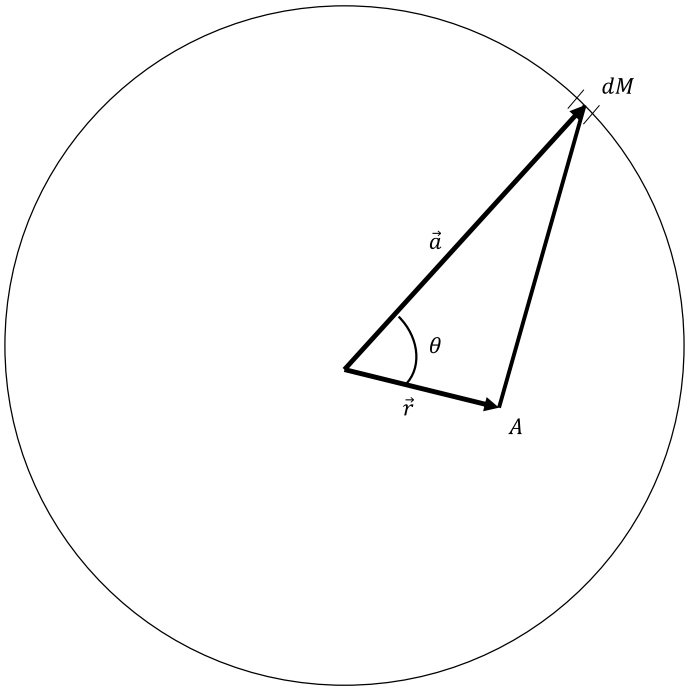

Figure 12: Calculating the potential of an infinitely thin ring on inside the plane

In this figure we see the method used to find the potential at an arbitrary point A inside a ring. First, we find the partial mass of the rind dM, and using the vectors $\vec{a}$ and $\vec{r}$, which point from the center of the ring to the point dM and A respectively, we find the partial potential from that point.

To find the potential at this arbitrary point, we find that the partial mass at dM is,

[23] Tatum, Jeremy. "Potential in the Plane of a Charged Ring." LibreTexts. February 22, 2017. Accessed April 10, 2018. https://phys.libretexts.org/TextMaps/Map:_Electricity_and_Magnetism_(Tatum)/2:_Electrostatic_Potential/2.2:_Potential_Near_Various_Charged_Bodies/2.2.6:_Potential_in_the_Plane_of_a_Charged_Ring.

$$dM = \frac{Md\theta}{2\pi} \tag{44}$$

To find the partial gravitational potential at this point, we see

$$d\Phi = \frac{-4\pi G}{4\pi}\frac{Md\theta}{2\pi}\frac{1}{\sqrt{a^2+r^2-2arcos(\theta)}} \tag{45}$$

We can simplify this to,

$$d\Phi = -\frac{GM}{2\pi a}\frac{d\theta}{\sqrt{1^2+\left(\frac{a}{r}\right)^2-2\frac{a}{r}cos(\theta)}} \tag{46}$$

Using the Legendre Polynomial expansion, we find the potential of this system is,

$$\Phi(\mathrm{r}) = \sum_{l=0}^{\infty}\left(A_l r^l + \frac{B_l}{r^{l+1}}\right)P_l(\cos(\theta)) \tag{47}$$

For r < a, we see that $\frac{B_l}{r^{l+1}} = 0$, so,

$$\Phi(\mathrm{r}) = \sum_{l=0}^{\infty}(A_l r^l)\,P_l(\cos(\theta)) \tag{48}$$

Now that we have found the potential of both the star and the disk, we can calculate the acceleration on a test partial caused by both. It is this value that will tell us if the disk has reached the reverse Roche limit, since, if the acceleration due to the disk is greater than the acceleration due to the star at the edge of the star, these partials will start to leave the stars surface. The acceleration is related to the gravitational potential with the equation,

$$\vec{a} = -\nabla\Phi \tag{49}$$

Thus, the tidal acceleration, which in this case is the same as the overall acceleration, of the sphere can be easily calculated. In spherical coordinates we see

$$\vec{a} = -\nabla\Phi = -\left(\left(\frac{\partial\Phi}{\partial \mathrm{r}}\hat{r}\right) + r\frac{\partial\Phi}{\partial\theta}\hat{\theta} + \frac{1}{rsin(\theta)}\frac{\partial\Phi}{\partial\phi}\hat{\phi}\right) \tag{50}$$

so the acceleration inside the sphere is,

$$\vec{a} = -\left(\frac{\partial}{\partial \mathrm{r}}\left(-GM\frac{\left(3{R_*}^2-r^2\right)}{2{R_*}^3}\right)\hat{r}\right)$$

$$= \frac{-GMr}{{R_*}^3}\hat{r} \tag{51}$$

Outside the sphere, the acceleration is,

$$\vec{a} = -\left(\frac{\partial}{\partial \mathrm{r}}\left(-\frac{GM}{r}\right)\hat{r}\right)$$

$$= \frac{-GM}{r^2}\hat{r} \tag{52}$$

Putting these together, we find that the acceleration due to the star in all space is,

$$\vec{a} = \begin{cases} \frac{-GMr}{{R_*}^3}\hat{r} & for\ r \le R_* \\ \frac{-GM}{r^2}\hat{r} & for\ r > R_* \end{cases} \tag{53}$$

Finding the acceleration of the disk is once again a little different then finding the acceleration of the star. Using equation 50, we know how to find the acceleration, but since it is a series, this can only be an approximation. However, despite the approximate nature of this calculation it is easy to calculate. In cylindrical coordinates the gradient is,

$$\vec{a} = -\nabla\Phi = -\left(\left(\frac{\partial\Phi}{\partial\rho}\hat{\rho}\right) + \frac{1}{\rho}\frac{\partial\Phi}{\partial\theta}\hat{\phi} + \frac{\partial\Phi}{\partial \mathrm{z}}\hat{\mathrm{z}}\right) \tag{54}$$

Since the potential of the disk within the plane is only dependent on the radial $\hat{\rho}$ direction, we see that the acceleration is simply,

$$\vec{a} = \frac{\partial}{\partial \mathrm{r}}\left(-\frac{GM}{2a}\left(1 + \frac{1}{4}\left(\frac{r}{a}\right)^2 + \frac{9}{64}\left(\frac{r}{a}\right)^4 + \frac{25}{256}\left(\frac{r}{a}\right)^6 + \frac{1225}{16384}\left(\frac{r}{a}\right)^8 + \cdots\right)\right) \tag{55}$$

This evaluates to,

$$\vec{a} = -\frac{GM}{2a}\left(\frac{1}{4a^2}r + \frac{9}{16a^4}r^3 + \frac{75}{128a^6}r^5 + \frac{1225}{2048a^8}r^7 + \cdots\right) \tag{56}$$

In order to find if a star disk system has exceeded the reverse Roche limit, we simply have to add the two acceleration equations together and see where this new equation evaluates to zero. If this radial value is below the value of the stars radius then the outer edges of the star will accelerate outward, resulting in the star ripping itself apart. This calculation is not trivial to do analytically, but it is trivial to computationally solve where this point will be by plotting the potential. The point of maximum potential will also be the point of zero acceleration, since $\vec{a} = -\nabla\Phi = -\frac{d\Phi}{d\varpi}$. Thus, where $\frac{d\Phi}{d\varpi}$ changes sign will be where $\vec{a}$ changes direction. First, let us look at distribution of potential in a simple system.

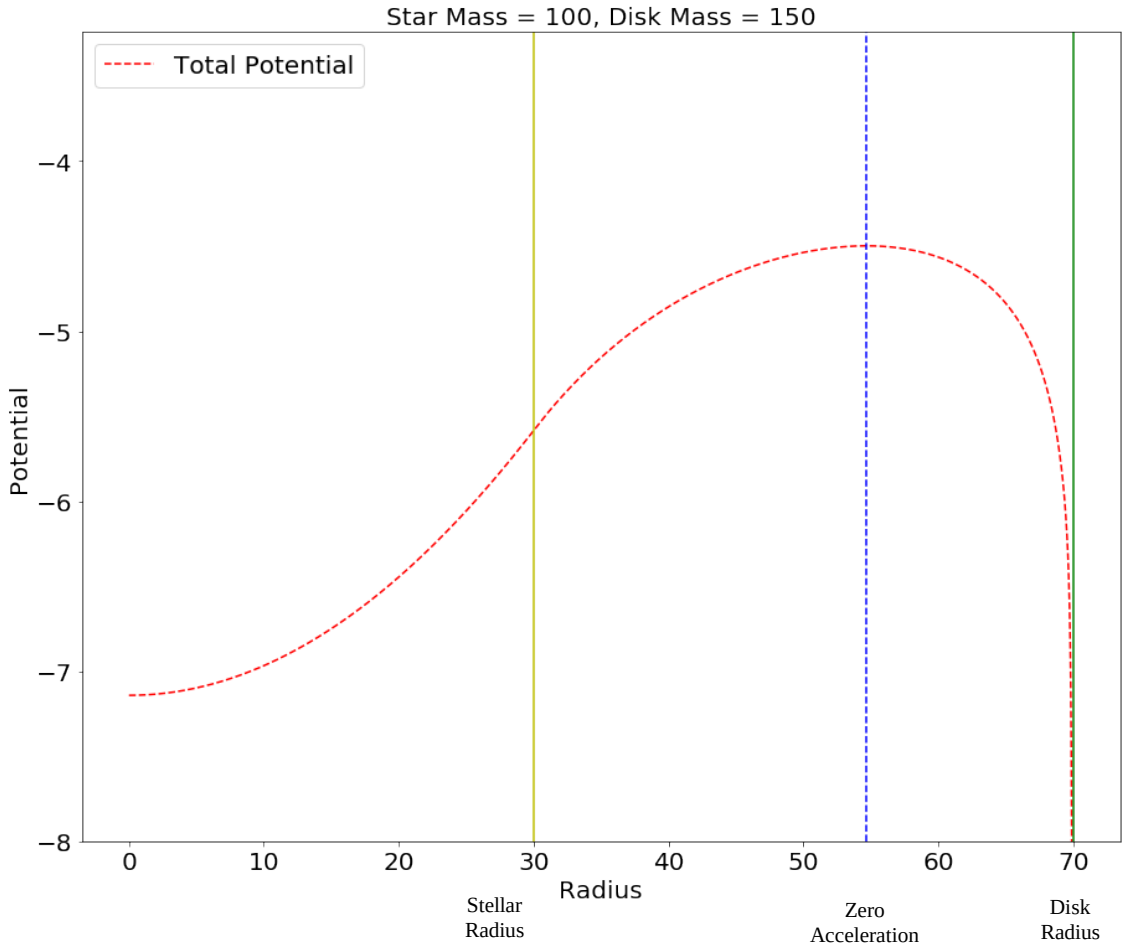

Figure 13: Total Potential of a Star Disk System

In this plot we see the total potential of a system with a mass ratio of 30, and a disk radius of 70, where these are some arbitrary unit. For this system, we see that the point of zero acceleration is much further out then the stars radius, so this is well outside the RRL.

In this simple test system, we see that for a star and ring of equal mass and a relatively large disk radius to star radius, the zero-acceleration point is far away from the surface of the star. This means that the stars structure will be minimally affected by the ring. By performing a series of these simple calculations, we are able to find the approximate value of the reverse Roche limit for any star-disk system.

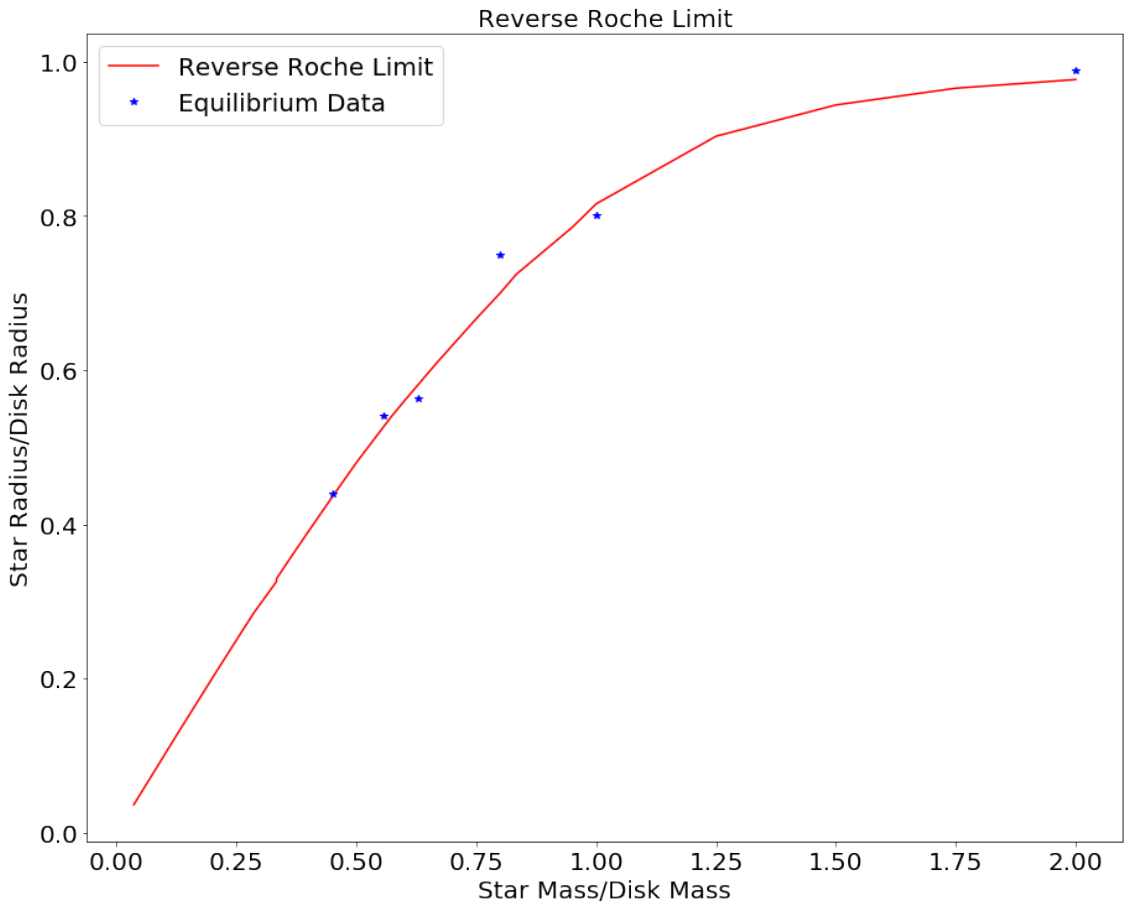

Figure 14: Reverse Roche Limit

In this plot we see the location of the reverse Roche limit as a function of the mass ratio and radius ratio of the star-disk system based on our simplified system. The blue stars are the reverse Roche limits in some of the equilibrium data sets. As we can see, these values closely match, but are not quite equal to the simple model.

At the end of this exercise we can now see that the method used to find the equilibrium conditions of our star-disk systems is consistent with a simplified version of this same problem. Stars that are shown to be at the brink of the reverse Roche limit in the modeling tool we use are also close to the same value calculated for a simple spherical star, with a simple ring. This shows that while much more complex, our model is showing the proper behavior for this system.

Part 3: Linear Analysis

The next step in our simulation is to take our results from our equilibrium models and start to evolve these initial systems in time. While we will eventually want to look at these with the *Chymera* code, modeling nonlinear systems is incredibly computationally expensive. Thus, it makes sence to find promising stars in a linear simulation. Specifically, we are trying to determine if the disk has any real effect on the fission process. Using our data collected in our equilibrium models, we will look at three stars from a given family group. The first star is one with a relatively large stellar mass to disk mass ratio. From looking at the families in figure 7, we see that this is where our data flattens out, approaching the angular velocity of a star without a ring. The second star is one close to the cutoff point. These are either stars that have reached their upper size limit for the size of ring given, or in most cases, stars that have almost reached the reverse Roche limit, and are close to being pulled apart by the gravitational

force of the disk. The third star is somewhere between these two extremes. We can see this selection process in figure 10.

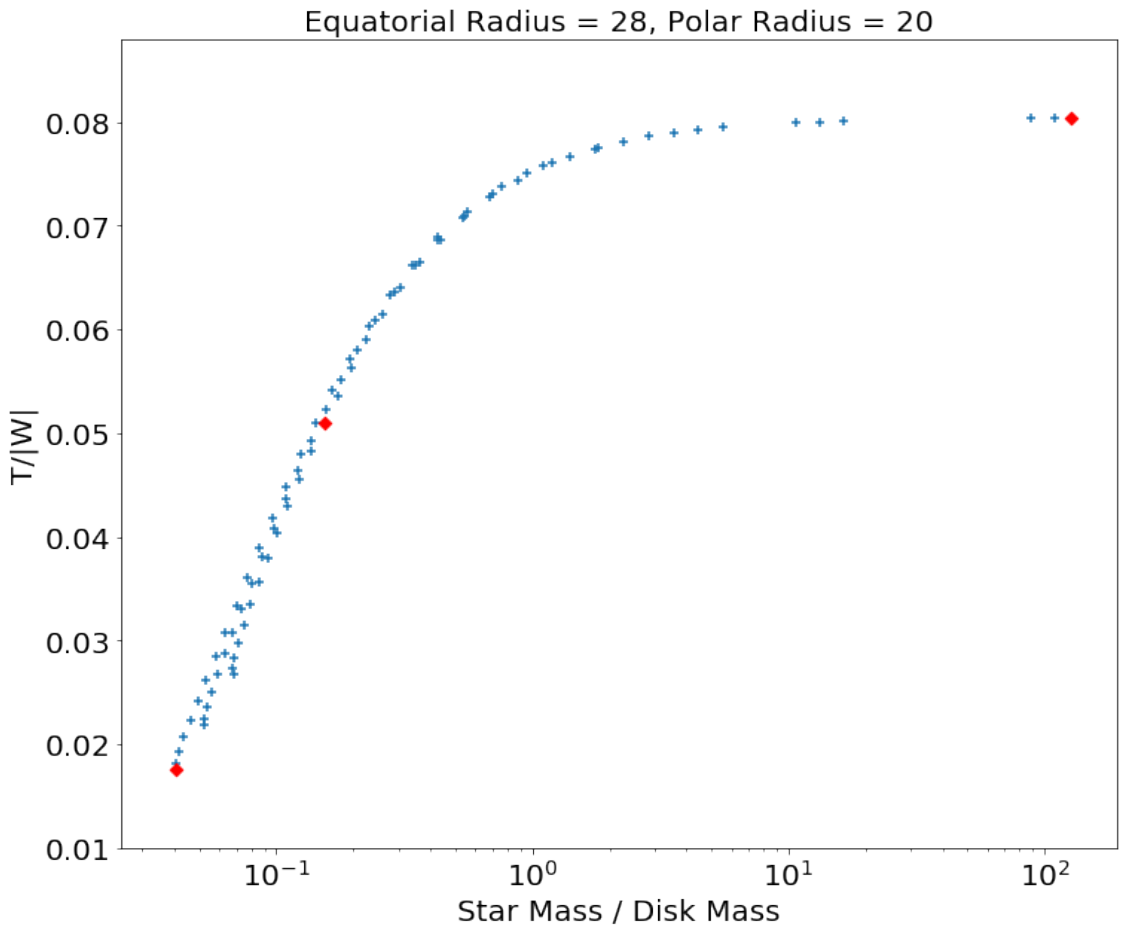

Figure 15: Selection of Linear Model Stars ($R_p = 20, R_{eq} = 28$)

In this plot we see the selected stars for one of our linear models. In this case, we are looking at the equilibrium data corresponding to stars with an equatorial radius of 28 and a polar radius of 20. We see that we have chosen three stars, with one corresponding to almost no ring, one with a ring approaching the reverse Roche limit, and one between these two extremes.

For our models, we have chosen to look at a wide variety of different stellar families. Besides the family seen in the figure above, we also looked at three stars from the other family groups in the 28-equatorial radius group; That being those with polar

radii of 12 and 4. We also looked at the 20-12, 84-20, 164-84 and 172-164 family groups. This gives us a wide range of stars with wildly varying initial conditions, with fast spinning stars with large differences in polar and equatorial radius, slow spinning nearly circular stars, and of course large variations in the size of each star. Each of these models takes several days to run, so we cannot simulate every star simulated in the equilibrium model, but these are a good representation of the population.

After we have completed our models, we must evaluate our data. Unfortunately, the linear model cannot tell us if the stars split into binary pairs. It is the inclusion of the nonlinear instabilities that we hope will allow this behavior. Even so, it is possible to tell if a star is likely to be stable or unstable. Let us look at the linear model for our star of equatorial radius, $R_{eq} = 28$, and polar radius, $R_p = 20$.

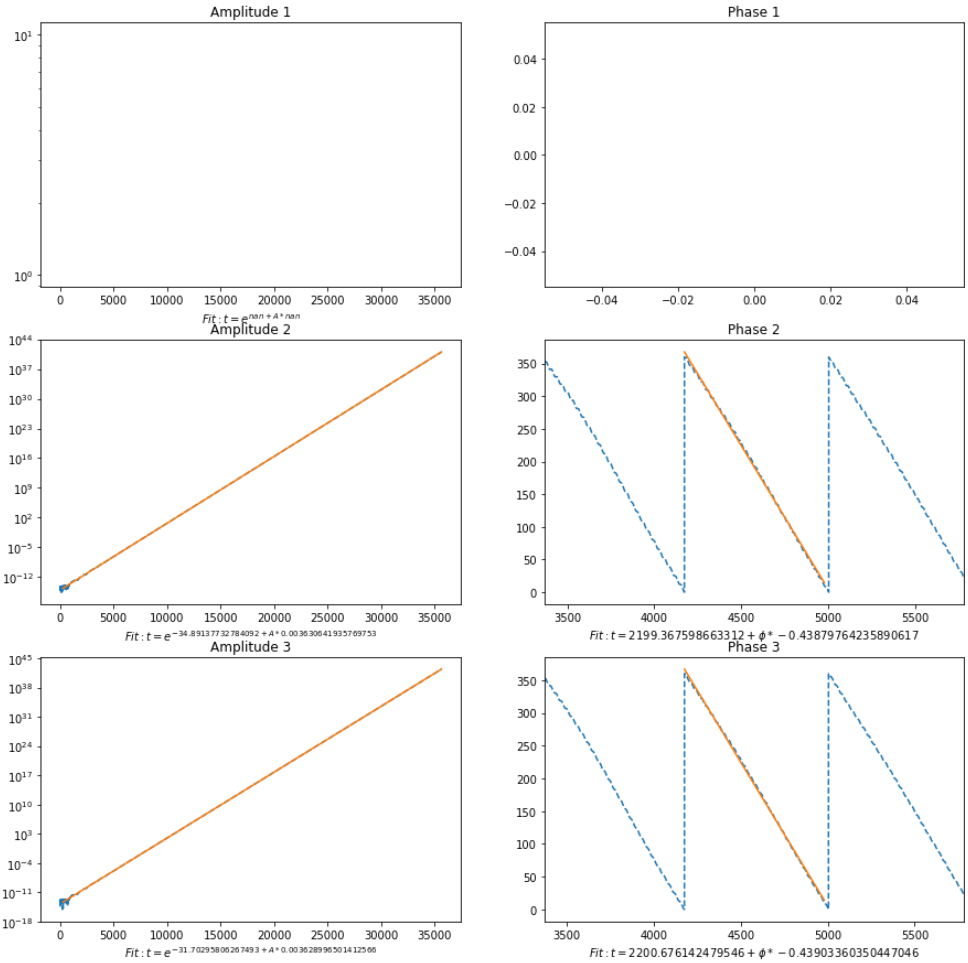

Figure 16: Amplitude and Phase data for Star (Approaching RRL)

In this plot we see amplitude and phase over time at three different radii. For clarity, the rate of growth for the second amplitude is $A = e^{t*0.0036}$, and $A = e^{t*0.0036}$ for the third amplitude. The phase osculation is changing by $\phi = -0.439 * t$ for the second phase and by $\phi = -0.439 * t$ for the third phase. For global modes, the growth rates and phases should be identical at each radius. To the extent that they differ, we estimate the uncertainties of our simulation.

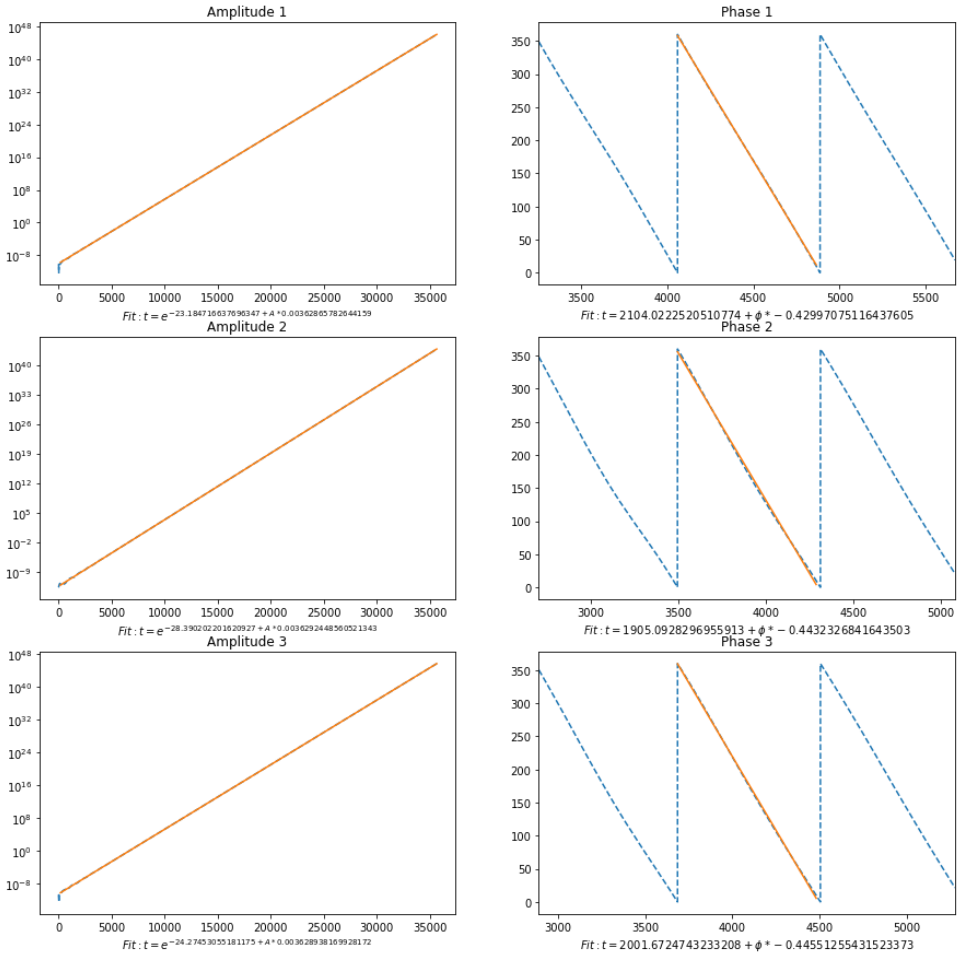

Figure 17: Amplitude and Phase data for Disk (Approaching RRL)

This plot is similar to the plot of the star amplitudes and phases. If we look at the amplitude data, we see after some time the value of the amplitude starts to grow exponentially. This is the rate of growth of the star or disk. Similarly, the phase data will go from almost random to sawtooth oscillations from 360 to 0. This tells us the rate at which the system is oscillating. For clarity, the rate of growth for the first amplitude is $A = e^{t*0.0036}$, the second is changing by $A = e^{t*0.0037}$ and the third is changing by $A = e^{t*0.0036}$. The phase osculation is changing by $\phi = -0.430 * t$ for the first, by $\phi = -0.443 * t$ for the second and by $\phi = -0.446 * t$ for the third phase.

When looking at this sample data, which is from the sample on the curve approaching the reverse Roche limit, we can tell that the system is unstable because of the exponential growth of the amplitude values. Let us compare this data to the sample taken with a minimal disk.

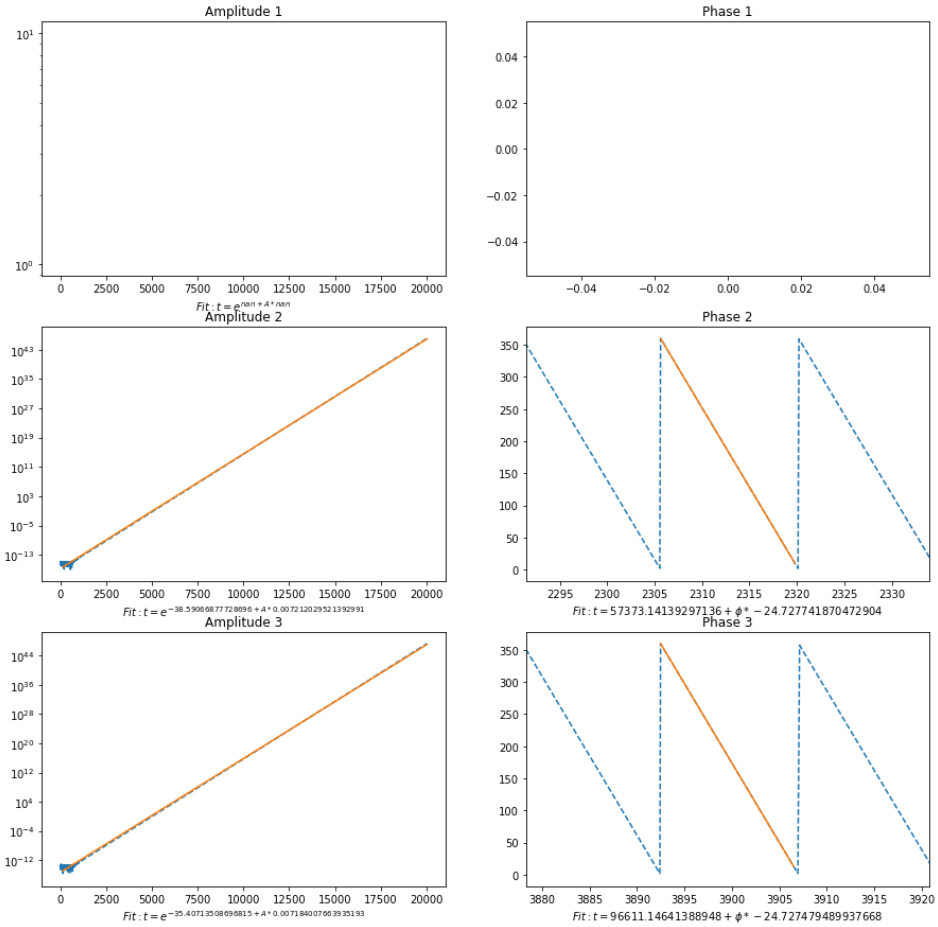

Figure 18: Amplitude and Phase data for Star (Far from RRL)

In this plot, we see the growth rate for a star far from the reverse Roche limit. Looking at the slopes for the second and third amplitude, we see that the star with the larger disk is evolving more slowly than the one with the smaller disk. Also, looking at the phase osculation, we see that the small disk is oscillating much more frequently. The rate of growth for the second amplitude is $A = e^{t*0.0072}$, and $A = e^{t*0.0072}$ for the third amplitude. The phase osculation is changing by $\phi = -24.7 * t$ for the second phase and by $\phi = -24.7 * t$ for the third phase.

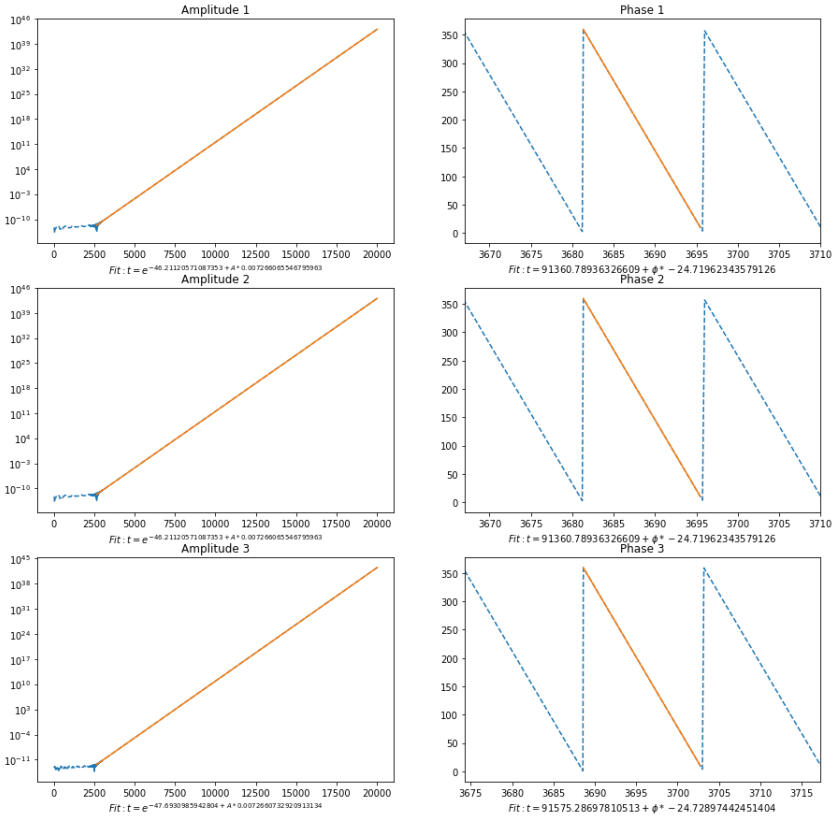

Figure 19: Amplitude and Phase data for Disk (Far from RRL)

In this plot we see that both the amplitude and phase plots are much different than those of the system approaching the RRL. The rate of growth is much smaller, and the oscillations are much quicker. The rate of growth for the first amplitude is $A = e^{t*0.0073}$, the second is changing by $A = e^{t*0.0073}$ and the third is changing by $A = e^{t*0.0073}$. The phase osculation is changing by $\phi = -24.7 * t$ for the first, by $\phi = -24.7 * t$ for the second and by $\phi = -24.7 * t$ for the third phase.

In these two plots we see how the ring has affected this system. The most obvious is that the sample with the large ring is evolving more slowly than the sample with the small ring. In binary formation, this will allow more time for nonlinear instabilities in the stellar structure to overcome linear instabilities trying to rip the star apart.

The other set of data we found in our equilibrium models noted here, was corresponding to the stars of polar radii, $R_p = 20$, and equatorial radii, $R_{eq} = 84$. This data was particularly interesting because the stars without a disk were immediately unstable, while the stars with a disk were driven below this threshold. This can be seen in the figure below.

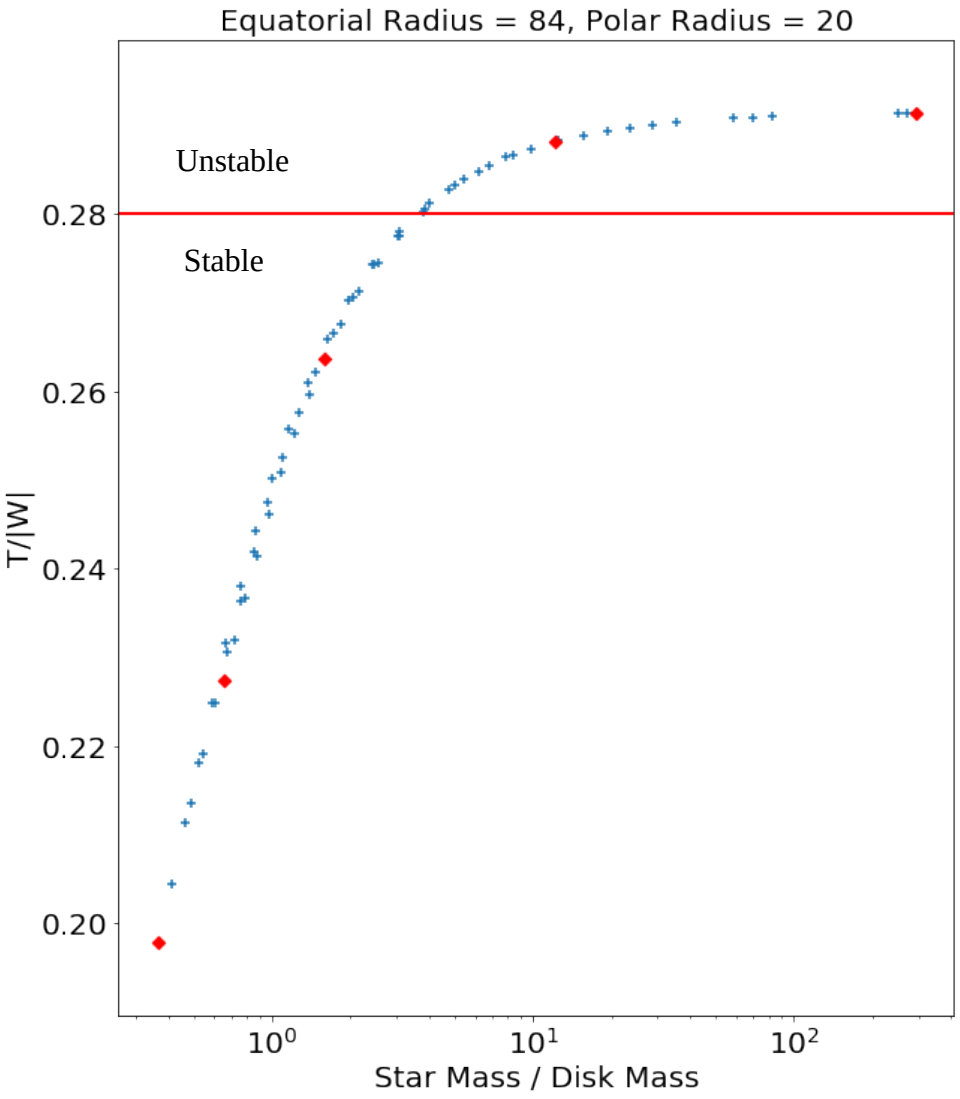

Figure 20: Selection of Linear Model Stars ($R_p = 20, R_{eq} = 84$)

In this plot we see the equilibrium model for a star of $R_p = 20$ and $R_{eq} = 84$. The red points indicate samples taken for use in the linear simulations. This set of samples is to test how a disk will affect stars that should be fundamentally unstable. $m = 2$

In this set of samples, we should see an increasing stability in our models as we approach the RRL, given that they have been driven over this instability threshold. After running our set of linear simulations, this is exactly what we see. Both of the samples above the threshold show that their disks were destroyed almost immediately and have growth rates between $A = e^{t*0.007}$ and $A = e^{t*0.011}$, which are quite high for this system. Alternatively, the samples below this threshold, while still becoming unstable quite quickly, do not show signs that their disks have collapsed, and have much slower growth rates of $A = e^{t*0.0036}$.

Star Radius Ratio (Equatorial Radius/Polar Radius)	Mode	Ratio (Star Mass/Disk Mass)	Rate of Growth 2 (exponential):	Phase Change 2:	Rate of Growth 3 (exponential):	Phase Change 3:
20/12	2	21.5	0.001890925	-0.83462501	0.001892102	-0.84172351
20/12	2	5.49	0.000683932	-0.07690806	0.000683932	-0.076908
20/12	2	0.432	0.00332125	-23.3090047	0.00332125	-23.3091302
28/4	2	5.02	0.000104857	-0.01043641	0.000104515	-0.01044127
28/4	2	1.33	0.000503679	-0.04661274	0.000501706	-0.04661274
28/4	2	0.0594	0.011434728	-1.04312316	0.011425751	-1.0461683
28/4	3	5.02	7.10E-05	-0.01603345	7.10E-05	-0.01603287
28/4	3	1.326	0.000400488	-0.07056402	0.000400488	-0.07056497
28/4	3	0.05938	0.009163789	-1.59163849	0.009163789	-1.59168084
28/12	2	4.47	0.949631653	-1.17125962	0.951084908	-1.17456066
28/12	2	0.347	0.003907702	-15.628735	0.003907702	-15.6286018
28/12	2	0.296	0.004571181	-18.291066	0.004571181	-18.2910331
28/12	3	4.472	0.946317594	-1.75790823	0.945889933	-2.11599427
28/12	3	0.3466	0.002484297	-0.51889267	0.002486415	-0.51902141
28/12	3	0.2961	0.002657286	-27.2381747	0.002657286	-27.2365613
28/20	2	7.07	0.007317199	-2.71852195	0.007317103	-2.7184786
28/20	2	1.07	0.003628022	-0.43567634	0.003627991	-0.435672
28/20	2	0.520	0.007266047	-24.7267007	0.007266047	-24.7278018
28/20	3	7.071	0.006600109	-5.3888695	0.00660903	-3.50873098
28/20	3	1.066	0.009228132	-6.13089579	0.00922777	-6.13145005
28/20	3	0.5196	0.004382731	-36.8986853	0.004382727	-36.7873235
84/20	2	0.322	0.008338246	-1.76900453	0.008338243	-1.77023701

84/20	2	0.234	0.011243214	-2.17647988	0.011243208	-2.17668861	
84/20	2	0.212	582.133347	n/a	582.133074	n/a	
84/20	2	0.159	n/a	-8.34423222	n/a	-8.45912176	
84/20	2	0.103	776.1759849	-2.58395522	776.1756209	-2.5831402	
84/20	3	0.234	0.008142635	-4.11340749	0.008147231	-3.97118285	
84/20	3	0.159	12.20432792	-12.141599	12.09966135	-12.838118	
84/20	3	0.153	12.84236197	-12.460153	12.78520104	-13.1647687	
164/84	2	0.3.9	39.50681391	-20.1628902	39.42037036	-19.6433206	
164/84	2	0.387	33.6344815	-24.4083281	33.5199569	-24.4083281	
164/84	2	0.385	33.656898	-20.7192008	33.66758091	-20.9302326	
172/164	2	0.677	0.105543122	-31.3262812	0.105547099	-31.2635766	
172/164	2	0.674	0.0728821	-20.5231546	0.072888385	-20.5240691	
172/164	2	0.6733	0.04742101	-16.7937321	0.047421024	-16.7938168	

Table 2: Linear Simulation Stellar Instability Data

This data tells us the conditions of the star after it becomes unstable, as seen in figure 16. The first column tells us the ratio of equatorial and polar radius of our spinning star. The second tells us the mode we are specifically looking at. The third column is the mass ratio between the star and the disk, and loosely determines how close the star is to the RRL. In all but one of our groups we used one at the RRL, one halfway up the curve, and one with a negligible disk. The forth, sixth and eighth rows are the exponential growth rate of the instability inside the star, while the third, fifth and seventh are the phase change. These are separated into their Fourier components.

Star Radius Ratio (Equatorial Radius/Polar Radius)	Mode	Star to Disk Mass Ratio (Star Mass/Disk Mass)	Rate of Growth 1 (exponential):	Phase Change 1:	Rate of Growth 2 (exponential):	Phase Change 2:	Rate of Growth 3 (exponential):	Phase Change 3:
20/12	2	21.5	0.001893113	-0.83825552	0.001888646	-0.75809551	0.001878093	-0.72028914
20/12	2	5.49	0.000683932	-0.07690799	0.000683932	-0.07690805	0.000683932	-0.07690801
20/12	2	0.432	0.00332125	-23.3082803	0.00332125	-23.3082803	0.00332125	-23.3082803
28/4	2	5.02	0.000104874	-0.01043636	0.000104874	-0.01043641	0.000104874	-0.01043629
28/4	2	1.33	0.000503937	-0.04634075	0.000503937	-0.04634081	0.000503937	-0.04634193
28/4	2	0.0594	0.011436441	-1.04616948	0.011436442	-1.04616202	0.011436441	-1.04615352
28/4	3	5.02	7.10E-05	-0.01603257	7.10E-05	-0.01603334	7.10E-05	-0.01594373
28/4	3	1.326	0.000400488	-0.07056431	0.000400488	-0.07056625	0.000400488	-0.07056543
28/4	3	0.05938	0.009163789	-1.59168722	0.009163789	-1.59167394	0.009163789	-1.59167598
28/12	2	4.47	0.952591795	-1.17079264	0.926050454	-1.17828129	0.950428854	-1.17699151
28/12	2	0.347	0.003907701	-15.642635	0.003907701	-15.7207578	0.003907701	-15.6213527
28/12	2	0.296	0.004571181	-18.2920012	0.004571181	-18.2920012	0.004571181	-18.2918031
28/12	3	4.472	0.955348282	-1.75649857	0.955356761	-2.2012869	0.955368503	-2.18152334
28/12	3	0.3466	0.002485982	-0.52006362	0.002486545	-0.51919003	0.002485977	-0.52284726
28/12	3	0.2961	0.002657286	-27.238116	0.002657286	-27.238116	0.002657286	-27.2377754
28/20	2	7.07	0.007312016	-2.71680106	0.007311378	-2.71860462	0.007310305	-2.71913641
28/20	2	1.07	0.003627894	-0.43281107	0.003627995	-0.44326878	0.003627888	-0.43995662
28/20	2	0.520	0.007266047	-24.7273835	0.007266047	-24.7273835	0.007266047	-24.7268177
28/20	3	7.071	0.006603533	-4.45074629	0.006589934	-4.35220809	0.006595975	-3.94958509
28/20	3	1.066	0.009229643	-6.21751783	0.009228786	-6.61943221	0.009228397	-5.7807445
28/20	3	0.5196	0.004382726	-36.8204632	0.004382726	-36.8204632	0.004382727	-36.820791
84/20	2	0.322	0.008338244	-1.76810975	0.008338244	-1.76812081	0.008338244	-1.76810855
84/20	2	0.234	0.011243212	-2.17630552	0.011243212	-2.17631206	0.011243212	-2.17629074
84/20	2	0.212	582.0507616	n/a	582.0207214	n/a	581.9766049	n/a
84/20	2	0.159	n/a	-8.36342706	n/a	-8.36683326	n/a	-8.45764735

84/20	2	0.153	12.7890771	-8.05288047	12.7890771	-8.05288047	12.78907661	-8.05288047
84/20	3	0.234	0.008150392	-4.23649385	0.008141414	-4.19756714	0.008134949	-4.01558419
84/20	3	0.159	12.33446552	-12.6581564	12.3346638	-12.6578728	12.33425021	-12.6888128
84/20	3	0.153	12.78592572	--12.741993	12.78592572	-12.741993	12.78591938	-12.741993
164/84	2	0.389	39.60287925	-19.742881	39.60285861	-19.742881	39.6027541	-19.742881
164/84	2	0.387	33.73725278	-20.0892401	33.73694327	-20.0892401	33.73168159	-20.0892401
164/84	2	0.385	33.84470174	-20.1607263	33.84470174	-20.1607263	33.8446978	-20.1607263
172/164	2	0.677	0.106598881	-31.2795626	0.10552692	-31.3138979	0.10546811	-31.3324917
172/164	2	0.674	0.072931222	-20.9787662	0.073029305	-20.6012342	0.072938116	-20.5901858
172/164	2	0.6733	0.047387844	-16.7818959	0.047387844	-16.7818959	0.047391961	-16.7756293

Table 3: Linear Simulation Disk Instability Data

This data set is in the same format as the stellar instability data, be is for the corresponding disk. Notice that unlike the stellar object, the disk has first order Fourier components.

In these data sets, we see a general trend where the rate of growth increases as we approach the RRL. We first see that models predicted to be stable based on single star studies turn out to be unstable. This is likely because the stars are destabilized by the presence of the massive disks. This is particularly evident in the 84/20 system where the growth explodes as we cross the m=2 limit. This shows, at least in linear simulations, that approaching the RRL has a positive impact on the prospect for fission, since a slower growth of linear instabilities will allow the fission to process more time to occur. Despite these promising results however, we must run these same initial conditions through the nonlinear *chymera* simulation to tell if these effects will truly result in fission.

Part 4: Nonlinear Analysis

One aspect of this project that has unfortunately not yet been completed is the nonlinear analysis of our full system. The original plan was to go through the linear simulations and find promising candidates to do a full simulation on. In the meantime, we started a similar set of simulations as the nonlinear samples where we found a

family group of stars and chose three samples approaching the reverse Roche limit. Due to time constraints on this project we were never able to start the second set of simulations with our sifted data, and the first set were not able to advance as far as we would have liked. However, we did manage to glean some information. Let us look at the simulation that was able to advance the furthest out of our three. This sample is of a star nearly at the reverse Roche limit according to our equilibrium model.

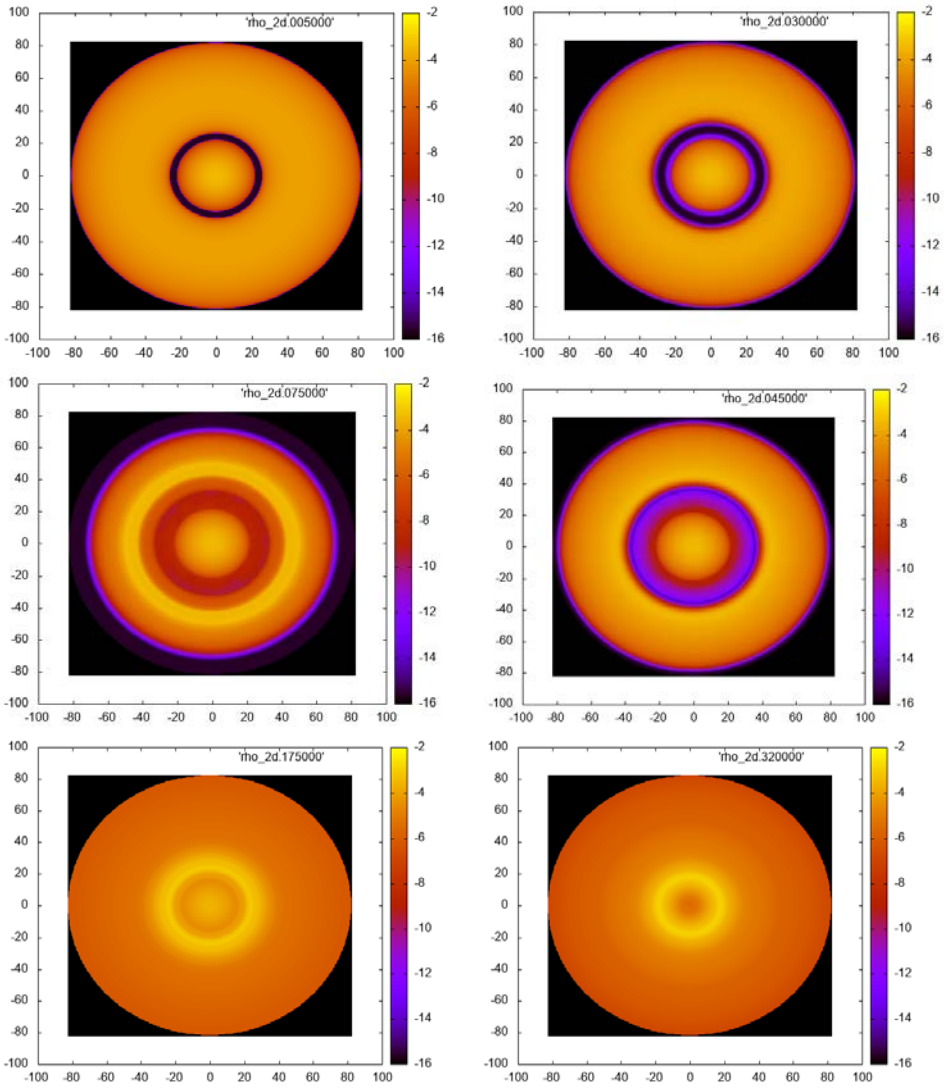

Figure 21: Star Disk Evolution

In this figure, we see the interaction between a star and disk in a nonlinear simulation. This particular case corresponds to a system midway through one of the family groups seen in the equilibrium models. In this case, the interaction between the disk and star increased over time, with pieces of both accelerating into one another. This lead to the merging to the outer edge of the star with the inner edge of the sphere, ultimately disrupting any bifurcation that might have been developing.

We see in this model that the disk and the star start pulling each other apart. The outer edge of the star starts to expand, leaving a much less dense material. At this point the two bodies start to accelerate toward one another, before merging. This interaction destabilizes any attempt by the star to fission. The remainder of the simulation shows the slow consumption of the disk by the central star. This destabilization is evident in the Fourier component plot of this simulation.

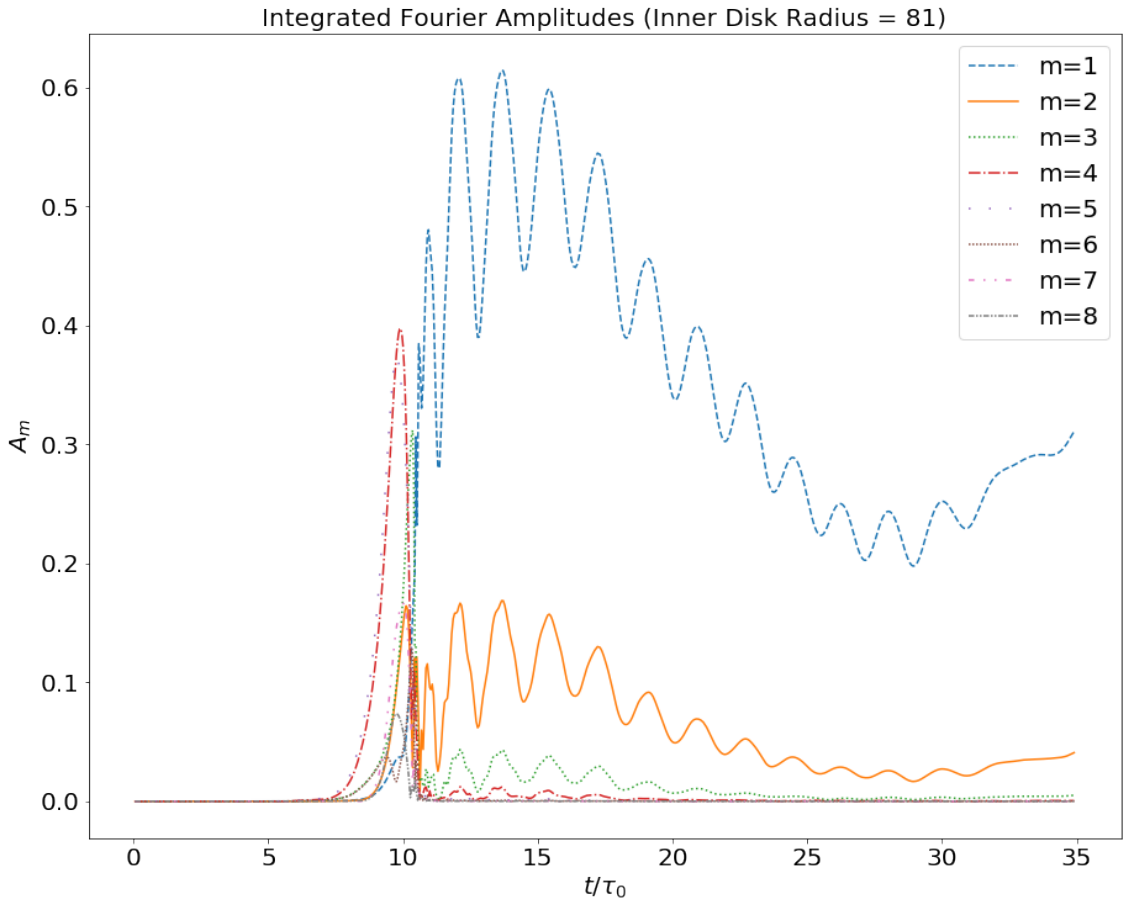

Figure 22: Fourier Component Plot for full Nonlinear Simulation

In this plot we see the Fourier components of the full nonlinear simulation. In this plot, we see that the fourth and fifth modes are the first to destabilize but are soon dominated by $m = 1$. This is characteristic of how the disk collapsed into the star, destabilizing the whole system.

While this was the only full nonlinear model we were able to complete, it does show some interesting differences to the linear simulation. In particular, we see that this system becomes unstable first in the $m = 4$ and $m = 5$ modes, before becoming dominated by the $m = 1$ mode. This is different from the linear simulations which were dominated by the $m = 2$ mode, and the solitary stars that were also dominated by the $m = 2$ mode. This makes intuitive sense for stars starting the fission process, as they stretch into a bar mode. However, the extreme nature of this system seems to have had

the effect of complicating the initial structure in such a way that the new modal structure could not remain stable. This is the most likely reason for the collapse of the disk and the breakup of the star. It would have been interesting to see if this behavior is typical of these systems, or just a special case, but that will have to wait until the completion of this project.

Chapter 4: Discussion

Part 1: Our Results

Throughout this project, it has been our goal to show the feasibility of the fission model. While I believe that our research could demonstrate this feasibility, we were not able to show this process in our simulations. It is unsurprising that the isolated rotating stars did not show this behavior, as these systems have been thoroughly simulated in the past, and have never given us our desired results, but in these simulations, we did see that the stars remained cohesive for much of their lifespan. It was only as the star started the fission process that material started to be flung off the main body. This does show that this model is not completely infeasible. However, the most striking evidence that we have found over the course of this project is the equilibrium data results. We see clearly from these simulations that the presence of a ring, particularly that of the stars with equatorial radius of 84 and polar radius of 20, drove what would have been unstable initial conditions into at least temporary stability. This gives stars with more extreme starting parameters a chance to fission. Also, based on the linear simulation, stars with medium to large rings have a slower growth rate when the ring and star do not merge early on. If these models were to be put through nonlinear evolution, I am confident that we would see, if not full binary formation, at least very different behavior to isolated stars with the same structure. I am excited to see how this research progresses after the conclusion of this project.

Part 2: Parallel Research

It is important to note at this time that this project was only part of a much larger continuing effort on the part of Doctor Imamura and his research team. I was merely a temporary addition to that team. While my research has focused primarily on exploring the limits of large disk systems, trying to find the effect of approaching the reverse Roche limit, the majority of our team's efforts have been looking into smaller disks with a wider range of stellar conditions. In particular, the work currently being done by Kathryn Hadley, William Dumas, Erik Keever, Rebecka Tumblin and of course my primary advisor Dr. James Imamura have already published a paper on this topic titled "Nonaxisymmetric Instabilities and Star-Disk Coupling I. Moderate Mass Disks". In this paper, the team looks at the interaction between a wide variety of stars in systems with a stellar mass to disk mass ratio of between $\frac{M_d}{M_*} = 0.2$ and 0.25. While still not observing clean binary separation, this research has shown that "coupling drives instabilities in slowly rotating stars" which would "otherwise be stable to dynamic nonaxisymmetric instabilities." Also, in some of our teams more recent simulations, we have seen what could be a clean binary separation in a star disk system. It is still too early to tell for sure, but it looks very promising.

We also plan on further investigating large disk systems like the ones primarily focused on in this paper in work by Hadley in 2018. Dr. Imamura's team has also been looking into the prospects of fragmentation of large circumstellar disks being the source of many short period binaries. While not complete, we have seen in some of our simulations the clean fragmentation of a narrow disk into separate bodies orbiting a central star.

The prospect that these objects could form stars is obviously only possible for the collapse of very massive disks, since small disks would not have the mass necessary to induce fusion in the cores of these objects. However, these early results seem promising.

Chapter 5: Conclusion

Binary star formation is one of the most interesting aspects of stars when looking into their structural dynamics. Despite our almost perfect understanding of nonrotating star formation, the solution to multi-star system formation remains a mystery. While the fragmentation model has had some success with long period binary formation, the two theories explaining short period binaries, tidal capture and fission, have been widely discounted. It was the purpose of this study to revisit the fission model with an up to date understanding of fluid dynamics and an increase in computation power to try to show the models feasibility. We also wanted to see what the effects of adding a large disk around the system would have as the effect of the disk approaching the reverse Roche limit started to pull the star apart. It is my opinion that we have been successful in this goal overall. While we were not able to see the clean bifurcation in our single star systems that we had hoped, we have at least given this new approach consideration. It seems that the nonlinear instabilities utilized in the *Chymera* code that were not known of during the last set of major simulations do not have any appreciable effect on this system.

What is more interesting to me is our results after we added a disk to the system. While these nonlinear simulations were largely unfinished by the end of this project, some of the early simulations show some promise. In particular, the stabilizing effects seen in large, rapidly rotating stars when inserted into massive disk systems show great promise. It is these systems that we hope to investigate further as this project continues. The linear simulations of the set of systems simulating stars of equatorial radius 84 and polar radius 20 in particular show great promise. Without a ring, these stars are always

going to be unstable. Their $T/|W|$ value will always fall above the threshold for stability. However, in our linear simulations we saw that this value was pushed down sufficiently to be initially stable. When evolved, we saw that the models with larger disks had significantly slower rates of growth, or the speed at which the instabilities grew in the system. This would theoretically give the stars in these systems more time to evolve, and fission. It was these models that we evolved in the nonlinear simulation, but unfortunately only the star with the most massive disk was thoroughly investigated. In this simulation we saw that the star, though initially stable, was slowly pulled apart by the disk. A more thorough investigation of the rest of our linear models will need to be made to determine if this is typical behavior or just the product of this extreme system. However, despite not quite finishing our simulations, we have seen behavior in some of our systems that could produce fission, and that in and of itself is enough to state that this model has not yet been disproven.

Bibliography

Alves, João F., Bruce G. Elmegreen, Josep Miquel. Girart, and Virginia Trimble. Computational star formation: proceedings of the 270th Symposium of the International Astronomical Union held in Barcelona, Catalonia, Spain, May 31-June 4, 2010. Cambridge, UK: Cambridge University Press, 2011.

Baldwin, Kyle A., Samuel L. Butler, and Richard J. A. Hill. "Artificial tektites: an experimental technique for capturing the shapes of spinning drops." Scientific Reports 5, no. 1 (2015). doi:10.1038/srep07660.

Boss, A. P. "Collapse, Equilibrium, and Fragmentation of Rotating, Adiabatic Clouds." *International Astronomical Union Colloquium* 58 (1980): 255-59. doi:10.1017/s0252921100081628.

Brusov, Peter N., and Paul P. Brusov. "Nonlinear Hydrodynamic Equations for Superfluid Helium in Aerogel." *Physics Letters A*314, no. 3 (2003): 239-43. doi:10.1016/s0375-9601(03)00877-6.

Carroll, Bradley W., and Dale A. Ostlie. *An introduction to modern astrophysics*. Harlow: Pearson, 2014.

Catelan, P., F. Lucchin, S. Matarrese, and L. Moscardini. "Eulerian Perturbation Theory in Non-flat Universes: Second-order Approximation." *Monthly Notices of the Royal Astronomical Society*1, no. 1 (1995). doi:10.1093/mnras/276.1.39.

Clarke, Cathie. "Theories for binary star formation." *Astrophysics and Space Science* 223, no. 1-2 (1995): 73-86. doi:10.1007/bf00989156.

Drazin, P. G., and W. H. Reid. Hydrodynamic Stability. Cambridge: Cambridge University Press, 2004.

Durisen, R. H., and J. E. Tohline. *Protostars and planets II*. Edited by Mildred Shapley. Matthews and David C. Black. Tucson, AZ: The University of Arizona Press, 1985, 534-575.

Durlevich, Olga. "General Catalogue of Variable Stars: Homepage." PINK FLOYD DISCOGRAPHY/ARCHIVE LIST. Accessed May 14, 2018. http://www.sai.msu.su/gcvs/gcvs/.

Faber, S. M., Ewine Fleur Van Dishoeck, and J. Kormendy. *Annual Review of Astronomy and Astrophysics: Volume 51, 2013*. Palo Alto, CA: Annual Reviews, 2013.

Geller, Aaron M., Jarrod R. Hurley, and Robert D. Mathieu. "Directn-Body Modeling Of The Old Open Cluster Ngc 188: A Detailed Comparison Of Theoretical And Observed Binary Star And Blue Straggler Populations." *The Astronomical Journal*145, no. 1 (2012): 8. doi:10.1088/0004-6256/145/1/8.

Godreche, Claude, and Paul Manneville. Hydrodynamics and Nonlinear Instabilites. Cambridge: Cambridge University Press, 1996.

Hadley, Kathryn Z., Paul Fernandez, James N. Imamura, Erik Keever, Rebecka Tumblin, and William Dumas. "Nonaxisymmetric instabilities in self-gravitating disks. II Linear and quasi-linear analyses." *Astrophysics and Space Science* 353, no. 1 (July 19, 2014): 191-222. doi:10.1007/s10509-014-1994-8.

HIRSCH, MORRIS W., Stephen Smale, and Robert L. Devaney. *DIFFERENTIAL EQUATIONS, DYNAMICAL SYSTEMS, AND AN INTRODUCTION TO CHAOS*. 3rd ed. S.l.: ELSEVIER ACADEMIC PRESS, 2017.

Howe, Alex. "Binary Star Formation: Dynamical Evolution." Https://www.astro.princeton.edu/~eco/AST541/Alex_Howe.pdf.

Kerswell, Richard R. "Elliptical Instability." *Annual Review of Fluid Mechanics* 34, no. 1 (2002): 83-113. doi:10.1146/annurev.fluid.34.081701.171829.

Kondo, Yoji, Ronald Sylvester. Polidan, and Roberto SisterÓ. Evolutionary processes in interacting binary stars: proceedings of the 151st Symposium of the International Astronomical Union, held in Cordoba, Argentina, August 5-9, 1991. Dordrecht: Kluwer academic publ., 1992.

Kratter, Kaitlin M. "The Formation of Close Binaries." *Harvard-Smithsonian Center for Astrophysics*, September 16, 2011.

Lacaze, Laurent, Patrice Le Gal, and Stéphane Le Dizès. "Elliptical instability of the flow in a rotating shell." Physics of the Earth and Planetary Interiors 151, no. 3-4 (2005): 194-205. doi:10.1016/j.pepi.2005.03.005.

Lass, Harry, and Leon Blitzer. "The Gravitational Potential Due to Uniform Disks and Rings." *Celestial Mechanics*30, no. 3 (1983): 225-28. doi:10.1007/bf01232189.

Lucy, L. B. "A Numerical Approach to the Testing of the Fission Hypothesis." *The Astronomical Journal*82 (1977): 1013. doi:10.1086/112164.

Lucy, L. B. "The Formation of Close Binaries." *Close Binary Stars: Observations and Interpretation*, 1980, 7-14. doi:10.1007/978-94-009-9038-8_2.

Ou, Shangli, Joel E. Tohline, and Patrick M. Motl. "Further Evidence for an Elliptical Instability in Rotating Fluid Bars and Ellipsoidal Stars." *The Astrophysical Journal* 665, no. 2 (2007): 1074-083. doi:10.1086/519785.

Pringle, J. E. "On the Formation of Binary Stars ." *Monthly Notices of the Royal Astronomical Society* 239 (July 18, 1989): 361-70. doi:10.1093/mnras/239.2.361.

Pringle, J. E. "Binary Star Formation." *The Physics of Star Formation and Early Stellar Evolution*, 1991, 437-48. doi:10.1007/978-94-011-3642-6_12.

Sahade, J., G. E. McCluskey, and Y. Kondo, eds. *The Realm of Interacting Binary Stars*. Vol. 177. Springer Netherlands, 1993.

Schulz, Norbert S. From dust to stars: studies of the formation and early evolution of stars. Berlin: Springer, 2007.

Strogatz, Steven H. Nonlinear Dynamics and Chaos: With Applications to Physics, Biology, Chemistry, and Engineering. 2nd ed. Reading, MA: Addison-Wesley Pub., 1994.

Tatum, Jeremy. "Potential in the Plane of a Charged Ring." LibreTexts. February 22, 2017. Accessed April 10, 2018. https://phys.libretexts.org/TextMaps/Map:_Electricity_and_Magnetism_(Tatum)/2:_Electrostatic_Potential/2.2:_Potential_Near_Various_Charged_Bodies/2.2.6:_Potential_in_the_Plane_of_a_Charged_Ring.

Tobin, John J., Leslie W. Looney, Zhi-Yun Li, Claire J. Chandler, Michael M. Dunham, Dominique Segura-Cox, Sarah I. Sadavoy, Carl Melis, Robert J. Harris, Kaitlin Kratter, and Laura Perez. "The Vla Nascent Disk And Multiplicity Survey Of Perseus Protostars (Vandam). Ii. Multiplicity Of Protostars In The Perseus Molecular Cloud." *The Astrophysical Journal*818, no. 1 (2016): 73. doi:10.3847/0004-637x/818/1/73.

Ward-Thompson, Derek, and Anthony P. Whitworth. *An introduction to star formation*. Cambridge: University Press, 2015.